Deep Space Network

214
Pseudo-Noise and Regenerative Ranging

Document Owner:		Approved by:	
Signature Provided	07/10/2023	Signature Provided	5/17/2023
Andrew O'Dea Telemetry, Tracking, and Command System Engineer	Date	Timothy Pham Communications Systems Chief Engineer	Date
Prepared By:		**Released by:**	
Signature Provided	05/11/2023	Signature Provided	08/03/2023
Peter Kinman Telecommunications Technical Consultant	Date	Christine Chang DSN Document Release Authority	Date

DSN No. **810-005, 214, Rev. C**
Issue Date: August 03, 2023
JPL D-19379; CL#23-3965

Jet Propulsion Laboratory
California Institute of Technology

Users must ensure that they are using the current version in DSN Telecommunications Link Design Handbook website: https://deepspace.jpl.nasa.gov/dsndocs/810-005/

Review Acknowledgment

By signing below, the signatories acknowledge that they have reviewed this document and provided comments, if any, to the signatories on the Cover Page.

Signature Provided	04/25/2023	Signature Provided	05/10/2023
Jeff Berner DSN Project Chief Engineer	Date	Scott Bryant DSN Ranging Cognizant Development Engineer	Date

Document Change Log

Rev	Issue Date	Prepared By	Affected Sections or pages	Change Summary
Initial	10/7/2003	P. W. Kinman	All	New Module
A	10/28/2015	P. W. Kinman	All	Added CCSDS range codes. Added curve fits for probability of acquisition. Added model for turn-around ranging channel with SDST AGC. Added performance comparison of PN and sequential ranging.
B	7/17/2019	P. W. Kinman	Many	Rewrote “Allocation of Link Power” section, including new models for downlink phase deviation for each of two types of turn-around ranging channels. Added new equation for chip rate. Added new information on DSS delay. Added glossary. Rewrote many paragraphs for improved clarity.
C	08/03/2023	P. W. Kinman	Sections 2.1, 2.2.1, 2.3, 2.3.2.1, 2.3.2.2, 2.5.2, 2.5.3, 2.5.3.1, 2.5.3.2, 2.5.4, 2.5.8 Figures 4, 10, 11	Modified Equation (34) of 214B, which is now Equation (40) of 214C. Added equations for filtering of feedthrough command by ranging channel. Added models for effect of interference on range measurement.

Contents

Illustrations

Figure **Page**

Tables

Table **Page**

1. Introduction

1.1 Purpose

This module describes capabilities of the Deep Space Network (DSN) for pseudo-noise (PN) ranging. These capabilities are available within the 70-m, the 34-m High Efficiency (HEF), and the 34-m Beam Waveguide (BWG) subnets. Performance depends on whether the spacecraft transponder uses a turn-around (non-regenerative) ranging channel or a regenerative ranging channel. Performance parameters are provided for both cases.

1.2 Scope

The material contained in this module covers the PN ranging system that may be utilized by both near-Earth and deep-space missions. This document describes those parameters and operational considerations that are independent of the particular antenna being used to provide the telecommunications link. For antenna-dependent parameters, refer to Module 101, 103, or 104 of this handbook. The other ranging scheme employed by the DSN is sequential ranging, described in Module 203.

An overview of the ranging system is given in Section 2.1. The parameters to be specified for ranging operations are explained in Section 2.2. The distribution of link power is characterized in Section 2.3. The spectrum of an uplink carrier modulated by a PN ranging signal is discussed in Section 2.4. The performance of turn-around and regenerative ranging is summarized in Section 2.5. Non-coherent ranging is also discussed there. Section 2.6 describes the corrections required to determine the actual range to a spacecraft. The total error for a range measurement is discussed in Section 2.7.

2. General Information

The ranging signal of interest in this module is a logical combination of a range clock and several PN codes; this signaling technique is called PN ranging. A different signaling technique, sequential ranging, is also supported by the DSN. The same instrumentation within the DSN supports both PN ranging and sequential ranging. However, there are performance differences between these two signaling techniques. This module only discusses PN ranging. Sequential ranging is discussed in Module 203.

A spacecraft transponder may have either a turn-around ranging channel or a regenerative ranging channel. The DSN processes a PN ranging signal in the same way for both types of transponder ranging channel. The performance of a PN range measurement will generally be better when the transponder uses a regenerative ranging channel. This module characterizes the performance of both regenerative ranging and non-regenerative (turn-around) ranging when the PN-ranging signaling technique is employed.

The range clock is coherently related to the carrier. The uplink carrier is often tuned during a tracking pass, in order to compensate for the Doppler effect on the uplink carrier, thereby reducing stress on the transponder's carrier-tracking loop. As the uplink carrier is tuned, the range-clock frequency varies proportionately.

In two-way ranging, one Deep Space Station (DSS) both transmits the uplink and receives the downlink. For two-way ranging, the user may calculate the round-trip light time (RTLT) from data provided by the DSN: phase measurements of the ranging signal and a record of the transmitted uplink carrier frequency.

Three-way ranging is also supported, for which one DSS transmits the uplink and a different DSS receives the downlink. As with two-way ranging, the DSN reports phase measurements of the ranging signal and a record of the uplink-carrier frequency. From these data, the user may calculate the light time for the travel of the ranging signal from the uplink DSS, through the spacecraft, to the downlink DSS.

To put matters in perspective, the measurements discussed here are phase measurements and the resulting data permit the user to calculate time delays. Range cannot be calculated directly and accurately from the time delays because the range changes significantly over the course of the signal travel time. Similar measurement techniques employed in terrestrial applications, where the distances and measurement times are much smaller, typically permit the calculation of the range as the two-way time delay times the speed of an electromagnetic wave divided by 2. That has been the justification for using the term range measurement for this class of measurement technique. The two-way and three-way time delays calculated for deep-space missions are useful in the orbit determination process. These calculated delays assist in the improvement of trajectory models; and so, indirectly, the delays assist in the estimation of range as a function of time.

It is customary to quote range measurement error in units of meters. For two-way ranging, the range error is defined as the error in the two-way time delay times the speed of electromagnetic waves in vacuum divided by 2. (The division by two accounts for the fact that range is a one-way distance but the time delay is two-way.)

2.1 System Description

The DSN ranging system records the phase of the ranging signal that is transmitted and measures the phase of the ranging signal that returns. For two-way ranging, both recorded phase values (that of the uplink ranging signal and that of the downlink ranging signal) apply to a common instant in time, an epoch of the 1-pulse per second timing reference, which becomes the common time tag. From the difference between the uplink and downlink phases and from the history of the transmitted range-clock frequency (which can be calculated from the history of the uplink-carrier frequency), a user may compute the RTLT (Reference 1). This two-way time delay applies to a signal arriving at the DSS at the instant specified by the time tag.

The architecture for the DSN ranging system is shown in Figure 1. The ranging signal originates in the Uplink Subsystem (UPL). The returned signal is processed in the Downlink Tracking and Telemetry Subsystem (DTT). Both the UPL and the DTT are located at the Deep Space Communications Complex (DSCC).

The signal processing in the UPL may be summarized as follows. The Uplink Signal Generator (USG) synthesizes the range clock such that it is coherently related to the uplink carrier. The range-clock frequency equals a rational factor times the uplink carrier frequency. The USG generates the ranging signal, which is the range clock modified by additional signal structure that makes possible resolution of the phase ambiguity. A sample of

the uplink phase, which is required for the delay measurement, is passed from the USG to the Uplink Processor Assembly (UPA). The USG modulates the uplink carrier with the ranging signal. The klystron supplies the final stage of power amplification for the uplink carrier.

The downlink carrier, after amplification within the Low-Noise Amplifier (LNA), passes to the DTT. Frequency down-conversion to an intermediate frequency (IF) takes place in the RF-to-IF Downconverter (RID). The IF signal is sent to an IF-to-Digital Converter (IDC). Demodulation of the IF carrier occurs in the Receiver, Ranging and Telemetry (RRT) processor. Also within the RRT, the correlation of the received, baseband ranging signal with a local model produces a measurement of the downlink phase. This downlink phase is passed to the Downlink Channel Controller (DCC).

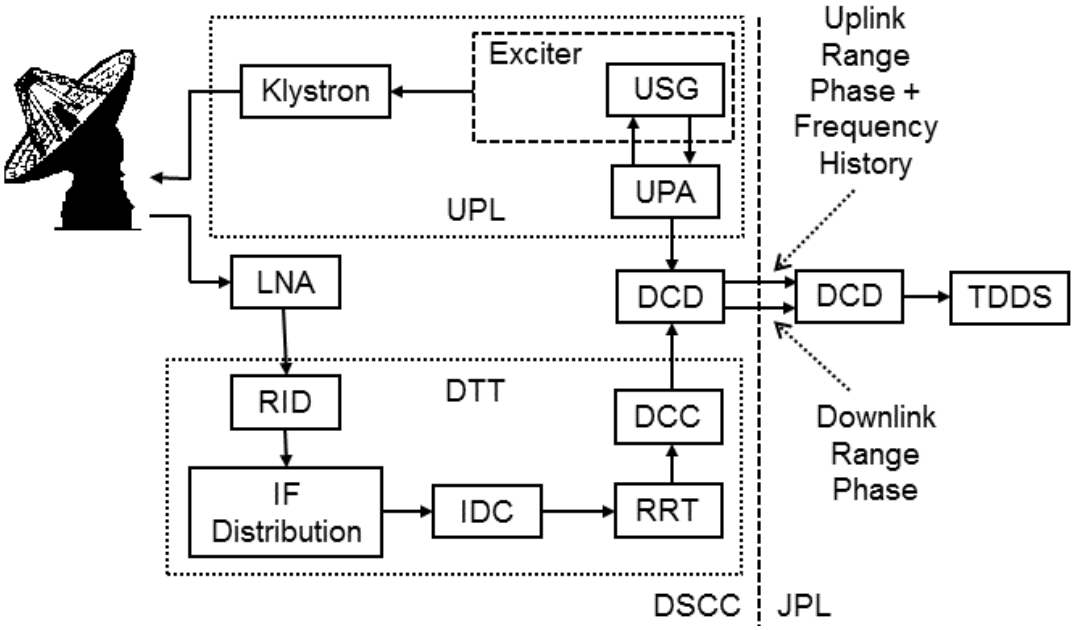

Figure 1. The DSN Ranging System Architecture

Uplink phase samples, each corresponding to an epoch of the 1-PPS (pulse per second) clock, are passed from the UPA, via the Data Capture and Delivery (DCD) software, to the Tracking Data Delivery Subsystem (TDDS), located in Pasadena. The DCC passes the downlink phase measurement and its time tag (an epoch of the 1-PPS clock), via the DCD, to the TDDS. A history of the uplink range clock's frequency is also needed for the calculation of the two-way time delay. Since the uplink range clock is coherently related to the uplink carrier, this necessary information can be derived from the history of the uplink carrier frequency, which is supplied by the UPA to the TDDS. All data required for the two-way delay calculation are archived by the TDDS for later use by a navigation team or other users.

The IDC, RRT, and DCC required for the processing of a downlink carrier are located within a Downlink Channel Processing Cabinet (DCPC). Each DCPC supports a single channel. For spacecraft with multiple channels (for example, X-band and Ka-band), or for

multiple spacecraft within a single antenna beamwidth, multiple DCPCs will be assigned to that antenna.

The DSN uses the Range Unit (RU) to deliver the difference of the ranging signal's uplink phase and downlink phase. Since the range clock and the carrier are coherently related, it is permissible to define the RU in terms of carrier phase. For an S-band uplink, the RU is defined as two cycles of the carrier. For an X-band uplink, one RU is $(749/221)$ times two cycles of the carrier. For a Ka-band uplink, one RU is $(3599/221)$ times two cycles of the carrier. Because the RU is defined with a factor (1 for an S-band uplink, $749/221$ for an X-band uplink, and $3599/221$ for a Ka-band uplink) that is proportional to frequency, the RU is proportional to time delay. (But the RU is a dimensionless unit.) One RU corresponds to approximately 0.94 ns of time delay.

A user may convert a two-way phase delay in RU into a two-way time delay as follows:

$$\text{Two-way Time Delay} = \begin{cases} \dfrac{2 \times RU}{f_S}, & \text{S-band uplink} \\ \dfrac{749}{221} \cdot \dfrac{2 \times RU}{f_X}, & \text{X-band uplink} \\ \dfrac{2407}{221} \cdot \dfrac{2 \times RU}{f_K}, & \text{K-band uplink} \\ \dfrac{3599}{221} \cdot \dfrac{2 \times RU}{f_{Ka}}, & \text{Ka-band uplink} \end{cases} \quad (1)$$

where f_S is the frequency of an S-band uplink carrier, f_X is the frequency of an X-band uplink carrier, f_K is the frequency of a K-band uplink carrier, and f_{Ka} is the frequency of a Ka-band uplink carrier. For example, if the uplink carrier is in the X band with a frequency of 7.16 GHz and the two-way phase delay is reported as 6,500,000 RU, then the two-way time delay is 6,153,467 ns.

2.2 Parameters Specified for Ranging Operations

The following subsections present the parameters that are required in ranging operations.

2.2.1 Chip Rate and Range-Clock Frequency

In the PN ranging system, the PN ranging signal is created by filtering a composite code, where timing is defined by the range clock. The chip rate f_{chip} for the composite code is defined in terms of a rational factor A/B (a ratio of two positive integers).

$$f_{\text{chip}} = \begin{cases} \dfrac{A}{B} \times f_S, & \text{S-band uplink} \\ \dfrac{221}{749} \times \dfrac{A}{B} \times f_X, & \text{X-band uplink} \\ \dfrac{221}{2407} \times \dfrac{A}{B} \times f_K, & \text{K-band uplink} \\ \dfrac{221}{3599} \times \dfrac{A}{B} \times f_{Ka}, & \text{Ka-band uplink} \end{cases} \tag{2}$$

f_S is the frequency of an S-band uplink carrier, f_X is the frequency of an X-band uplink carrier, f_K is the frequency of a K-band uplink carrier, and f_{Ka} is the frequency of a Ka-band uplink carrier. A/B is defined, in turn, by the whole numbers l_{CR} and k_{CR} (Reference 2).

$$\frac{A}{B} = \frac{l_{CR}}{128 \cdot 2^{k_{CR}}} \tag{3}$$

The chip rate is coherently related to the uplink carrier frequency, as suggested by Equation (2). l_{CR} and k_{CR} are whole numbers that together determine the rational factor A/B relating f_{chip} to the uplink carrier frequency. Table 1 lists the selections for l_{CR} and k_{CR}. This table also indicates the approximate value of the chip rate that corresponds to each pair of whole numbers l_{CR} and k_{CR}. The exact chip rate depends, as indicated in Equation (2), on the uplink carrier frequency (and, therefore, on the channel assignment and on any Doppler compensation that may be done on the uplink).

The range clock is a periodic signal. Each half-cycle of the range clock corresponds to one chip. Therefore, the range-clock frequency f_{RC} equals one-half of the the chip rate f_{chip}.

$$f_{RC} = \frac{f_{\text{chip}}}{2} \tag{4}$$

The approximate value of f_{RC} is given in Table 1 for numbers pairs l_{CR} and k_{CR} of that table. The exact value of f_{RC} depends on the uplink carrier frequency.

The DTT receiver uses the range clock in two ways. First, the phase of the range clock is measured; this determines the accuracy of the range measurement. Second, the receiver achieves chip synchronization using the range clock; this is a necessary precursor to resolving the ambiguity.

2.2.2 Ranging Signal Structure

In the PN ranging system, a filtered composite code is used for ranging. The timing of the composite code is set by the range clock. Three different composite codes are available: the DSN range code, the CCSDS T4B code, and the CCSDS T2B code. Each of these composite codes is built from a common set of component codes. The three composite codes differ from each other because of the manner in which the component codes are combined.

Table 1. CCSDS Chip Rates

l_{CR}	k_{CR}	A/B	Approximate value of f_{chip}	Approximate value of f_{RC}
94*	6	47/4096	24 MHz	12 MHz
64	6	1/128	16 MHz	8 MHz
32	6	1/256	8 MHz	4 MHz
16	6	1/512	4 MHz	2 MHz
12	6	3/2048	3 MHz	1.5 MHz
11	6	11/8192	2.8 MHz	1.4 MHz
10	6	5/4096	2.6 MHz	1.3 MHz
9	6	9/8192	2.3 MHz	1.15 MHz
8	6	1/1024	2 MHz	1 MHz
7	6	7/8192	1.8 MHz	900 kHz
6	6	3/4096	1.5 MHz	750 kHz
5	6	5/8192	1.3 MHz	650 kHz
4	6	1/2048	1 MHz	500 kHz
3	6	3/8192	750 kHz	375 kHz
2	6	1/4096	500 kHz	250 kHz
1	6	1/8192	250 kHz	125 kHz
2	8	1/16384	128 kHz	64 kHz
2	9	1/32768	64 kHz	32 kHz
2	10	1/65536	32 kHz	16 kHz

*This rate is used by the Bepi-Colombo mission and is outside defined CCSDS rates

2.2.2.1 Component Codes

Table 2 lists the component codes. In this table, a component code is represented as a finite-length sequence of bits. The length of the *n*-th component code is denoted λ_n for $1 \leq n \leq 6$. The lengths are: $\lambda_1 = 2$, $\lambda_2 = 7$, $\lambda_3 = 11$, $\lambda_4 = 15$, $\lambda_5 = 19$, and $\lambda_6 = 23$. (The first component code is the 2-bit sequence representing the range clock.) The *n*-th component code is denoted $b_n(i)$, where i represents a discrete-time index, $0 \leq i < \lambda_n$. The proper order of each of

these component codes is determined by reading the bits in each row from left to right. So, for example, the first three bits of $b_3(\cdot)$ are all 1s and the final bit is a 0.

It is also useful to represent each component code as a sequence of chips (with the bi-polar values ± 1).

$$c_n(i) = 2\, b_n(i) - 1 \tag{5}$$

where $c_n(i) = \pm 1$. Equation (5) translates a binary 1 into $+1$ and a logical 0 into -1.

Table 2. Component Codes

b_n	code	λ_n
b_1	1, 0	2
b_2	1, 1, 1, 0, 0, 1, 0	7
b_3	1, 1, 1, 0, 0, 0, 1, 0, 1, 1, 0	11
b_4	1, 1, 1, 1, 0, 0, 0, 1, 0, 0, 1, 1, 0, 1, 0	15
b_5	1, 1, 1, 1, 0, 1, 0, 1, 0, 0, 0, 0, 1, 1, 0, 1, 1, 0, 0	19
b_6	1, 1, 1, 1, 1, 0, 1, 0, 1, 1, 0, 0, 1, 1, 0, 0, 1, 0, 1, 0, 0, 0, 0	23

2.2.2.2 DSN Range Code

The DSN range code (also called the JPL range code) was the first composite code to be implemented and validated with the current ranging instrumentation in the DSN. Following is an explanation of how this composite code is generated from the component codes listed in Table 2.

For each finite-length PN code $b_n(i)$, a periodic code $b_n{}'(i)$ of period λ_n is formed by endless repetition:

$$b_n{}'(i) = b_n(i \bmod \lambda_n) \tag{6}$$

where $b_n{}'(i)$ is binary valued. In this document, the prime ($'$) indicates a periodic sequence (made from a finite-length sequence by periodic extension).

The composite code is

$$b'(i) = b_1{}'(i) \cup [b_2{}'(i) \cap b_3{}'(i) \cap b_4{}'(i) \cap b_5{}'(i) \cap b_6{}'(i)] \tag{7}$$

where $\cup$ and $\cap$ are the logical OR and logical AND operators, respectively. Since the component code lengths λ_n ($1 \le n \le 6$) are relatively prime, the period L (in bits) of the composite code is the product of the component code lengths. That is,

$$b'(i+L) = b'(i) \tag{8}$$

where

$$L = \prod_{n=1}^{6} \lambda_n = 1{,}009{,}470 \tag{9}$$

The periodic chip sequence corresponding to the periodic bit sequence $b'(i)$ is

$$c'(i) = 2\,b'(i) - 1 \tag{10}$$

where $b'(i)$ is the periodic bit sequence of Equation (7). $c'(i)$ is bi-polar, $c'(i) = \pm 1$.

In this design a large *L* is obtained from relatively small component code lengths. A large *L* is necessary for resolution of the range ambiguity, yet small λ_n are needed for a practical implementation of the correlators at the receiver. The ambiguity resolution of this code is given by

$$\text{ambiguity resolution} = \frac{c \cdot L}{4 f_{RC}} \tag{11}$$

where f_{RC} is the range-clock frequency and c is the speed of electromagnetic waves in vacuum. For a range clock of approximately 1 MHz, the ambiguity resolution is 75,660 km.

An important property of this composite code is that it approximates a sequence of period 2 bits. The composite code equals ${b_1}'(i)$, the first component with a period of 2 bits, most of the time. The effect of the other 5 component codes is to invert a small fraction (1/32) of the logical 0s in ${b_1}'(i)$. Since ${b_1}'(i)$ corresponds to the range clock, the composite code may be viewed as the range clock with an occasional inversion of a logical 0.

Most of this ranging signal's power lies at the range-clock frequency. This is desirable, since the accuracy of the range measurement is set by a correlation against a local model of the range clock. The occasional inversion is necessary to resolve the range ambiguity, but for this purpose the inversions need not be frequent.

2.2.2.3 CCSDS T4B Code

The Consultative Committee for Space Data Systems (CCSDS) recommends a composite code called T4B for use in deep-space ranging (Reference 2). The T4B code employs the same set of component codes that are used by the DSN range code (Table 2). The T4B code is constructed from the component chip sequences:

$${c_n}'(i) = c_n(i \bmod \lambda_n) \tag{12}$$

where $c_n(\cdot) = \pm 1$ is the chip sequence of length λ_n for the n-th component code, as given by Equation (5), and ${c_n}'(\cdot)$ is its periodic extension. The periodic, composite chip sequence $c'(i)$ is computed from the components ${c_n}'(i)$ as follows:

$$c'(i) = \text{sign}[4{c_1}'(i) + {c_2}'(i) - {c_3}'(i) - {c_4}'(i) + {c_5}'(i) - {c_6}'(i)] \tag{13}$$

where $c'(i) = \pm 1$ and where sign[·] is the algebraic sign of its argument. The period of the composite code $c'(i)$ equals L, as given in Equation (9). The ambiguity resolution of this code is the same as that for the DSN range code; this resolution is given in Equation (11).

As suggested by Equation (13), the range clock ${c_1}'(i)$ has a disproportionate influence on the composite code $c'(i)$. The composite code may be viewed as the range clock with an occasional inversion of a chip. (With the T4B code, unlike the DSN range code, the inversion may go in either direction: $-1 \rightarrow +1$ or $+1 \rightarrow -1$.) As with the DSN range code, most of the ranging signal's power lies at the range-clock frequency. As shown in Section 2.5, the performance of the T4B code is close to that of the DSN range code.

2.2.2.4 CCSDS T2B Code

The CCSDS recommends a second composite code, called T2B, which provides an alternative to the T4B code in performance trade-off space (Reference 2). The T2B code employs the same set of component codes (Table 2) that are used by the DSN range code and the T4B code. The periodic, composite chip sequence $c'(i)$ for the T2B code is computed from the components ${c_n}'(i)$ as follows:

$$c'(i) = \text{sign}[2{c_1}'(i) + {c_2}'(i) - {c_3}'(i) - {c_4}'(i) + {c_5}'(i) - {c_6}'(i)] \qquad (14)$$

The period of the T2B code equals L, as given in Equation (9). The ambiguity resolution of this code is the same as that for the T4B code and the DSN range code; this resolution is given in Equation (11).

In the construction of the T2B code, using Equation (14), the range clock ${c_1}'(i)$ gets only 2 "votes", whereas in the construction of the T4B code, using Equation (13), the range clock gets 4 "votes". As a result, the T2B code places less power in the range clock. The T2B code will therefore generally produce a less accurate range measurement than the T4B code; however, the T2B code will achieve a better probability of acquisition for smaller received power levels.

2.2.2.5 PN Ranging Signal

The PN ranging signal is created by filtering the composite code. This is accomplished with the uplink ranging filter, which is digitally implemented within the USG. The uplink ranging filter is a low-pass filter with a configurable bandwidth. The default (and minimum) bandwidth is 1.2 MHz. The PN ranging signal, available at the output of the uplink ranging filter, is used to phase-modulate the uplink carrier. This modulation also happens in the USG.

The purpose of the uplink ranging filter is to limit the bandwidth of the modulated uplink carrier. Because phase modulation is a non-linear modulation, the bandwidth of a carrier that is phase-modulated by the PN ranging signal can be much wider than twice the bandwidth of the PN ranging signal. If the composite code were not low-pass filtered, but instead sent directly to the phase modulator, the bandwidth of the uplink carrier would, in general, be much wider yet. (The command signal, if present, also contributes to the bandwidth of the uplink carrier, but typically the command signal has a much smaller bandwidth than the PN ranging signal. The PN ranging signal, when present, is therefore the modulating signal that plays the dominant role in determining the bandwidth of the uplink carrier.)

The bandwidth of the uplink ranging filter has a default value of 1.2 MHz. This is also the minimum bandwidth. This filter can be configured for a larger bandwidth. For a range-clock frequency larger than 1 MHz, it will be necessary to use a larger bandwidth. The decision about what bandwidth to use will be based, in part, on the effect of the filter on the PN ranging signal but also must account for spectral occupancy of the uplink carrier.

The composite code, as it appears at the input to the uplink ranging filter, is a sequence of bi-polar chips, where each chip is represented by a rectangular pulse. The uplink ranging filter will remove the highest-frequency content from this chip stream, so the PN ranging signal at the filter output will have slower transitions and smooth features. In the case where the uplink ranging filter passes the fundamental harmonic of the range clock but blocks third and higher-order harmonics of the range clock, a square-wave range clock on the filter input becomes a sinewave range clock on the filter output. The composite code on the filter input becomes on the filter output, in this case, a sequence of bi-polar chips, where each chip may be represented approximately by a half-cycle of a sinewave. This is illustrated in Figure 2 for the first eight chips of the DSN range code. The parameter T_c is the chip period. The range-clock frequency equals $1/(2T_c)$. This is the desired situation for the purpose of minimizing the spectral occupancy of the uplink carrier.

The range clock is modeled, in this module, as a sinewave. The PN ranging signal is modeled as the composite code but with each chip a half-cycle of a sinewave, as depicted in Figure 2. These models are good approximations when the uplink ranging filter passes the fundamental harmonic of the range clock but blocks the third harmonic (and higher-order harmonics) of the range clock. Even if this condition is not strictly met, these models are useful as first-order approximations; they lead to performance equations that may be easily calculated. Trying to get more accurate results would typically involve computer simulations.

There is also the limiting case where the bandwidth of the uplink ranging filter is much larger than the range-clock frequency. In this limit, the range clock is a square-wave and the PN ranging signal is the composite code (with chips represented by rectangular pulses). This limiting case is only approached when the range-clock frequency is much smaller than 400 kHz (one-third of 1.2 MHz). Since the accuracy of the range measurement improves with increasing range-clock frequency, this scenario is not common.

2.2.3 Integration Time

The integration time *T* should be large enough that the probability of range measurement acquisition is close to 1.0 and the range error due to downlink thermal noise is small (see Section 2.5). In the special case of non-coherent ranging, the presence of a frequency mismatch between the received ranging signal and the local model means that there is also reason to keep *T* relatively small, so that an optimum *T* should be carefully chosen for non-coherent ranging.

2.2.4 Uplink Ranging Modulation Index

The uplink ranging modulation index is chosen to get a suitable distribution of power among the ranging and command sidebands and the residual carrier on the uplink (see Section 2.3). With turn-around (non-regenerative) ranging, the uplink ranging modulation index also affects the distribution of power on the downlink carrier. The analysis appearing below

employs an rms phase deviation of the uplink carrier. This rms phase deviation equals the peak modulation index divided by $\sqrt{2}$ for the usual case of a sinewave range clock.

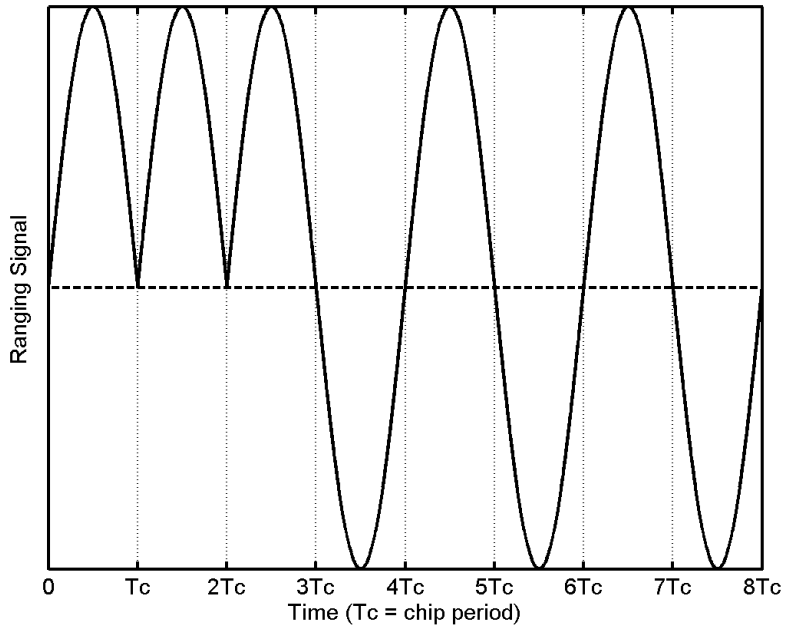

Figure 2. PN Ranging Signal When Third Harmonic of Range Clock is Blocked

2.2.5 Tolerance

The tolerance plays a role in deciding whether to judge range acquisitions as "in lock" or "out of lock". The ranging process does not use a phase-locked loop, so ranging lock status is estimated using the ranging probability of acquisition. For any given range acquisition, the ratio P_R/N_0 of the downlink ranging signal power to the noise spectral density is measured. From this measured P_R/N_0, an estimate of the probability of acquisition P_{acq} is calculated. Section 2.5 describes the calculation of the P_{acq} from P_R/N_0.

Tolerance may be selected over the range of 0.0% to 100.0%. The default value for tolerance is 99%. An acquisition lock status depends upon the following criteria:

$P_{\text{acq}}(\%) \geq$ Tolerance *results in* Acquisition declared "in lock"

$P_{\text{acq}}(\%) <$ Tolerance *results in* Acquisition declared "out of lock"

This procedure is explained for the example where the tolerance has the default value of 99%. For a given acquisition, P_R/N_0 is measured. From this measured value, the probability of acquisition P_{acq} is calculated; this number is the probability that the ambiguity is correctly resolved for this particular acquisition. Treating P_{acq} as a percentage, it is compared with the tolerance of 99%. If $P_{\text{acq}}(\%)$ equals or exceeds 99%, the acquisition is declared "in lock". Otherwise, it is declared "out of lock". Note that the "out of lock" ranging data may be valid data, with a probability of $P_{\text{acq}}(\%)$ of being correct.

2.3 Allocation of Link Power

The power allocation for a link is the distribution of power among the important link components: the residual carrier, the ranging sidebands, and the data (command or telemetry) sidebands. The following notation is used here for both the uplink and downlink:

P_C = power in residual carrier

P_R = usable power in ranging sidebands

P_D = usable power in data sidebands

P_T = total link power

P_C is the power in a single spectral line at the carrier frequency. When P_C is finite (greater than zero), carrier synchronization may be obtained at the receiver using a phase-locked loop that tracks this residual carrier. (Carrier synchronization may also be obtained with a Costas loop tracking the data sidebands, which are symmetrically located about the nominal carrier frequency.)

P_R is that portion of the power in the ranging sidebands that is used in the range measurement. P_R includes both the spread-spectrum content arising from the PN code components as well as the two discrete spectral lines (at f_{RC} Hz above and at f_{RC} Hz below the residual carrier) that correspond to the range clock's fundamental harmonic. Higher-order harmonics (beyond the fundamental harmonic) of the range clock are not used in a range measurement and are not included in P_R. The range measurement error is determined by the discrete spectral lines of the range clock's fundamental harmonic. Ambiguity resolution is achieved using the spread-spectrum content.

For the uplink, P_D is that portion of the power in the command sidebands that is employed in command detection in the transponder. In the most common signal design for a deep-space uplink, command data modulate a sinewave subcarrier and P_D only accounts for the power in the sidebands associated with the upper and lower fundamental harmonic of the subcarrier frequency. In the case of a sinewave subcarrier, the higher-order harmonics of the subcarrier frequency are not employed in command detection in the typical transponder and are not included in P_D.

For some missions, the command signal is bi-polar. The term "bi-polar" can mean either NRZ or bi-phase (Manchester encoded) pulses; for both of these pulse shapes, each symbol is conveyed using one of two algebraically opposite (antipodal) pulse shapes. An example of bi-polar commanding is when the command symbols, represented as NRZ or bi-phase pulses, directly phase-modulate the uplink carrier. In this case, the uplink P_D accounts for all power in command sidebands, since the command detection process in the typical transponder utilizes all command sidebands arising from a bi-polar command signal.

For the downlink, P_D is that portion of the power in the telemetry sidebands that is employed in telemetry detection at the station. Commonly, the telemetry signal is bi-polar. The term "bi-polar" can mean either NRZ or bi-phase (Manchester encoded) pulses; for both of these pulse shapes, each symbol is conveyed using one of two algebraically opposite (antipodal) pulse shapes. An example of bi-polar telemetry is when the telemetry symbols, represented as NRZ or

bi-phase pulses, directly phase-modulate the downlink carrier or when these symbols modulate a square-wave subcarrier that, in turn, phase-modulates the downlink carrier. In such cases, all of the power in the telemetry sidebands is employed in telemetry detection. This is a result of both the data and the subcarrier (if present) being bi-polar.

For some missions, the telemetry signal modulates a sinewave subcarrier and this composite signal phase-modulates the downlink carrier. In such a case, the downlink P_D is that portion of the power in the telemetry sidebands that is employed in telemetry detection at the station. Not included is the power in the higher-order harmonics of the subcarrier frequency.

P_T is not, in general, the sum of P_C, P_R, and P_D. In general, P_T is larger than that sum. There are multiple reasons for this. First, P_R does not account for power in the higher-order harmonics of the sinewave range clock. Second, when multiple signals (for example, a ranging signal and a telemetry signal) simultaneously phase-modulate a carrier, intermodulation products arise. These intermodulation products consume link power but do not contribute to either the range measurement or telemetry detection. Moreover, for the downlink, noise sidebands are present (in the case of turn-around ranging).

In calculating power allocations for a modulated carrier, it is necessary to characterize the level of the modulation. In this document, the root-mean-square (rms) phase deviation of the carrier will be used for this purpose. The following symbols are used in this module to represent rms phase deviation of the carrier:

uplink:	ϕ_r	=	rms phase deviation by ranging signal, rad rms
uplink:	ϕ_{cmd}	=	rms phase deviation by command signal, rad rms
downlink:	θ_{rs}	=	rms phase deviation by ranging signal (strong signal), rad rms
downlink:	θ_r	=	rms phase deviation by ranging signal, rad rms
downlink:	θ_{cmd}	=	rms phase deviation by feedthrough command signal, rad rms
downlink:	θ_n	=	rms phase deviation by noise, rad rms
downlink:	θ_{tlm}	=	rms phase deviation by telemetry signal, rad rms

On the uplink, ϕ_r and ϕ_{cmd} are parameters, constant for any given tracking pass. For a sinewave range clock, ϕ_r is related to the peak modulation index for uplink ranging by:

$$\phi_r = (\text{peak modulation index for uplink ranging, rad})/\sqrt{2} \tag{15}$$

When a sinewave subcarrier is used with command, ϕ_{cmd} is related to the peak modulation index for command by:

$$\phi_{cmd} = (\text{peak modulation index for command, rad})/\sqrt{2}, \quad \begin{matrix}\text{sinewave}\\ \text{subcarrier}\end{matrix} \tag{16}$$

However, for a bi-polar command signal, ϕ_{cmd} equals the peak modulation index for command.

On the downlink, θ_{rs} is a constant parameter that is determined by the AGC in the turn-around ranging channel. θ_{rs} is the rms phase deviation of the downlink carrier by the ranging signal in a strong-signal scenario. In such a scenario, the noise in the transponder's ranging channel is negligible compared with the ranging signal and there is no command. This

scenario occurs in a test facility before flight and in the early phase of flight when the ranging signal-to-noise ratio in the transponder's ranging channel is large. For a sinewave range clock, θ_{rs} is related to the peak modulation index (strong signal) by:

$$\theta_{rs} = (\text{strong-signal peak modulation index for downlink ranging, rad})/\sqrt{2} \qquad (17)$$

When PN ranging is done with a turn-around (non-regenerative) ranging channel, the variables θ_r, θ_{cmd} and θ_n become important. Within a turn-around channel the uplink carrier is demodulated, and the baseband signal plus noise that is the result of this demodulation is presented to a filter. The filter output is applied to an automatic gain control (AGC) circuit. The signal plus noise that exits the turn-around ranging channel is phase-modulated onto the downlink carrier.

For an arbitrary signal-to-noise ratio in a turn-around ranging channel, the rms phase deviation by ranging signal on the downlink, denoted θ_r, is less than or equal to θ_{rs}. Thus, θ_r is a variable, depending on both the parameter θ_{rs} and the ranging signal-to-noise ratio in the ranging channel. θ_{rs} is the limiting value of θ_r, corresponding to the strong-signal case. If command is present on the uplink and that command passes through the transponder's ranging channel, then θ_r also depends on the command signal-to-noise ratio in the ranging channel.

Uplink noise passes through the ranging channel and is phase-modulated onto the downlink carrier. θ_n is the rms phase deviation by this ranging-channel noise. θ_n, like θ_r, is a variable that depends on both the parameter θ_{rs} and the ranging signal-to-noise ratio (and, possibly, also the command signal-to-noise ratio) in the ranging channel.

θ_{tlm} is the rms phase deviation of the downlink carrier due to telemetry. When the telemetry signal is bi-polar, the rms phase deviation and the peak modulation index for telemetry are identical. When a sinewave subcarrier is used with telemetry, θ_{tlm} is related to the peak modulation index for telemetry by:

$$\theta_{tlm} = (\text{peak modulation index for telemetry, rad})/\sqrt{2}, \quad \begin{matrix}\text{sinewave}\\ \text{subcarrier}\end{matrix} \qquad (18)$$

2.3.1 Uplink

The equations of this subsection represent the case where a ranging signal and a command signal are simultaneously present on the uplink carrier. The range clock is taken here to be a sinewave. The ratio of P_C to P_T, the carrier suppression, is

$$\left.\frac{P_C}{P_T}\right|_{\mathrm{U/L}} = J_0{}^2\left(\sqrt{2}\,\phi_r\right) \cdot S_{cmd}(\phi_{cmd}) \qquad (19)$$

The ratio of P_R to P_T is

$$\left.\frac{P_R}{P_T}\right|_{\mathrm{U/L}} = 2J_1{}^2\left(\sqrt{2}\,\phi_r\right) \cdot S_{cmd}(\phi_{cmd}) \qquad (20)$$

The ratio of the fundamental command sideband power to P_T is

$$\left.\frac{P_D}{P_T}\right|_{\mathrm{U/L}} = J_0{}^2\left(\sqrt{2}\,\phi_r\right) \cdot M_{cmd}(\phi_{cmd}) \tag{21}$$

where $J_0(\cdot)$ and $J_1(\cdot)$ are Bessel functions of the first kind of order 0 and 1, respectively. These functions are plotted in Figure 3. When the argument x of $J_0(x)$ and $J_1(x)$ is small and positive, the following approximations may be used:

$$J_0(x) \cong 1, \qquad 0 \le x \ll 1 \tag{22}$$

$$J_1(x) \cong x/2, \qquad 0 \le x \ll 1 \tag{23}$$

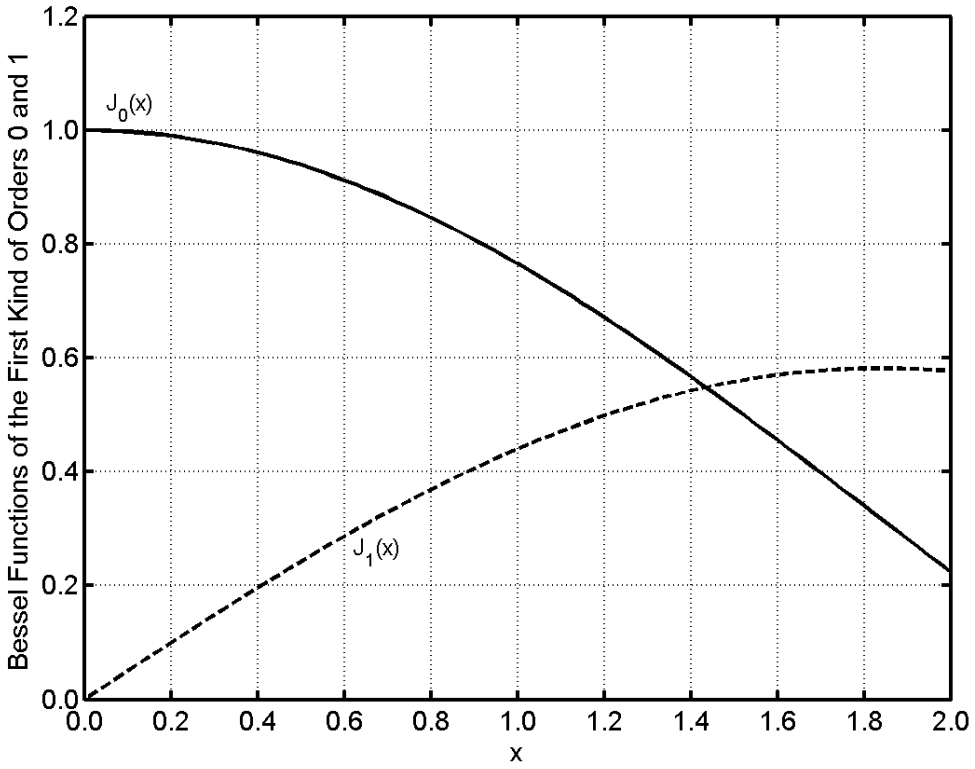

Figure 3. Bessel Functions of the First Kind of Order 0 and 1

The suppression factor $S_{cmd}(\phi_{cmd})$ in Equations (19) and (20) and the modulation factor $M_{cmd}(\phi_{cmd})$ in Equation (21) depend on whether the command signal is bi-polar or uses a sinewave subcarrier. These two factors are given by:

$$S_{cmd}(\phi_{cmd}) = \begin{cases} \cos^2(\phi_{cmd}), & \text{bi-polar} \\ J_0{}^2\left(\sqrt{2}\,\phi_{cmd}\right), & \text{sinewave subcarrier} \end{cases} \tag{24}$$

$$M_{cmd}(\phi_{cmd}) = \begin{cases} \sin^2(\phi_{cmd}), & \text{bi-polar} \\ 2{J_1}^2\left(\sqrt{2}\,\phi_{cmd}\right), & \text{sinewave subcarrier} \end{cases} \tag{25}$$

In the event that command is absent from the uplink, the factor $S_{cmd}(\phi_{cmd})$ in Equations (19) and (20) can be omitted, since $S_{cmd}(0) = 1$.

2.3.2 Downlink

The equations for power allocation on the downlink depend on whether the transponder has a turn-around (non-regenerative) ranging channel or a regenerative ranging channel.

2.3.2.1 Turn-Around (Non-Regenerative) Ranging

A turn-around ranging channel demodulates the uplink carrier, filters the baseband signal, applies automatic gain control, and then re-modulates the baseband signal onto the downlink carrier. The AGC serves the important purpose of ensuring that the downlink carrier suppression is approximately constant, independent of received uplink signal level. The bandwidth B_R of the transponder's ranging channel must be larger (typically about 50% larger) than the range-clock frequency, in order to pass the ranging signal with minimal distortion. For example, B_R is typically about 1.5 MHz when the transponder is intended to accommodate a range clock of 1 MHz. Substantial thermal noise from the uplink also passes through this channel. In many deep space scenarios, the thermal noise dominates over the ranging signal in this wideband, turn-around channel. Moreover, command signal from the uplink may pass through this ranging channel. In general, then, noise and command signal as well as the desired ranging signal are modulated onto the downlink carrier whenever the ranging channel is active (Reference 3).

The equations of this subsection represent the case where a ranging signal, a (feedthrough) command signal and noise are simultaneously present in the ranging channel, so that all three of these components, plus telemetry, phase-modulate the downlink carrier. The range clock is taken here to be a sinewave. The ratio of P_C to P_T, the carrier suppression, is

$$\left.\frac{P_C}{P_T}\right|_{\mathrm{D/L}} = {J_0}^2\left(\sqrt{2}\,\theta_r\right) \cdot S_{fth}(\theta_{cmd}) \cdot e^{-{\theta_n}^2} \cdot S_{tlm}(\theta_{tlm}) \tag{26}$$

The ratio of P_R to P_T is

$$\left.\frac{P_R}{P_T}\right|_{\mathrm{D/L}} = 2{J_1}^2\left(\sqrt{2}\,\theta_r\right) \cdot S_{fth}(\theta_{cmd}) \cdot e^{-{\theta_n}^2} \cdot S_{tlm}(\theta_{tlm}) \tag{27}$$

The ratio of the telemetry sideband power to P_T is

$$\left.\frac{P_D}{P_T}\right|_{\mathrm{D/L}} = {J_0}^2\left(\sqrt{2}\,\theta_r\right) \cdot S_{fth}(\theta_{cmd}) \cdot e^{-{\theta_n}^2} \cdot M_{tlm}(\theta_{tlm}) \tag{28}$$

The ratio of the command-feedthrough power to P_T is

$$\left.\frac{P_{fth}}{P_T}\right|_{\mathrm{D/L}} = J_0{}^2\left(\sqrt{2}\,\theta_r\right) \cdot M_{fth}(\theta_{cmd}) \cdot e^{-\theta_n{}^2} \cdot S_{tlm}(\theta_{tlm}) \tag{29}$$

where $J_0(\cdot)$ and $J_1(\cdot)$ are Bessel functions of the first kind of order 0 and 1, respectively.

The command-feedthrough suppression factor $S_{fth}(\theta_{cmd})$ that appears in each of Equations (26), (27) and (28) depends on whether the command signal is bi-polar or uses a sinewave subcarrier. This factor is given by:

$$S_{fth}(\theta_{cmd}) = \begin{cases} \cos^2(\theta_{cmd}), & \text{bi-polar} \\ J_0{}^2\left(\sqrt{2}\,\theta_{cmd}\right), & \text{sinewave subcarrier} \end{cases} \tag{30}$$

In the event that command feedthrough is absent from the ranging channel, the factor $S_{fth}(\theta_{cmd})$ in each of Equations (26), (27) and (28) can be omitted, since $S_{fth}(0) = 1$.

The command-feedthrough modulation factor $M_{fth}(\theta_{cmd})$ in Equation (29) depends on whether the command is bi-polar or uses a sinewave subcarrier. This factor is given by:

$$M_{fth}(\theta_{cmd}) = \begin{cases} \sin^2(\theta_{cmd}), & \text{bi-polar} \\ 2J_1{}^2\left(\sqrt{2}\,\theta_{cmd}\right), & \text{sinewave subcarrier} \end{cases} \tag{31}$$

The telemetry suppression factor $S_{tlm}(\phi_{tlm})$ in Equations (26), (27), and (29) and the telemetry modulation factor $M_{tlm}(\phi_{tlm})$ in Equation (28) depend on whether the telemetry signal is bi-polar or uses a sinewave subcarrier. These two factors are given by:

$$S_{tlm}(\theta_{tlm}) = \begin{cases} \cos^2(\theta_{tlm}), & \text{bi-polar} \\ J_0{}^2\left(\sqrt{2}\,\theta_{tlm}\right), & \text{sinewave subcarrier} \end{cases} \tag{32}$$

$$M_{tlm}(\theta_{tlm}) = \begin{cases} \sin^2(\theta_{tlm}), & \text{bi-polar} \\ 2J_1{}^2\left(\sqrt{2}\,\theta_{tlm}\right), & \text{sinewave subcarrier} \end{cases} \tag{33}$$

For a turn-around ranging channel, the downlink rms phase deviations θ_r, θ_n, and (if command feedthrough is present) θ_{cmd} depend on the ranging signal-to-noise ratio ρ_r and (if command feedthrough is present) the command signal-to-noise ratio ρ_{cmd} in the ranging channel.

$$\rho_r = \left.\frac{P_R}{P_T}\right|_{\mathrm{U/L}} \cdot \left.\frac{P_T}{N_0}\right|_{\mathrm{U/L}} \cdot \frac{1}{B_R} \tag{34}$$

$$\rho_{cmd} = \left.\frac{P_D}{P_T}\right|_{\mathrm{U/L}} \cdot \left.\frac{P_T}{N_0}\right|_{\mathrm{U/L}} \cdot \frac{1}{B_R} \cdot C_R(B_R T_{cmd}) \tag{35}$$

where

$P_T/N_0|_{\mathrm{U/L}}$ = uplink total power to noise spectral density ratio, Hz

B_R = noise-equivalent (one-sided) bandwidth of ranging channel, Hz

$C_R(B_R T_{cmd})$ = fraction of command-signal power passing through ranging channel

T_{cmd} = command symbol period (reciprocal of command symbol rate), s

The factor $C_R(B_R T_{cmd})$, which is limited by $0 \leq C_R(B_R T_{cmd}) \leq 1$, accounts for the fact that some of the command-signal power might not pass through the transponder's ranging channel. This factor is a function of the product $B_R T_{cmd}$. If most of the command signal passes through the ranging channel, then the factor $C_R(B_R T_{cmd})$ may be approximated as 1.

With high-rate command, the factor $C_R(B_R T_{cmd})$ can be significantly less than 1. Models are given here for $C_R(B_R T_{cmd})$ in the case of bi-polar command (with either NRZ or bi-phase pulses) that directly phase-modulates the uplink carrier.

When high-rate command signaling consists of NRZ pulses that directly phase-modulate the uplink carrier, $C_R(B_R T_{cmd})$ may be modeled as

$$C_R(B_R T_{cmd}) = 2T_{cmd} \int_0^{B_R} \frac{\sin^2(\pi f T_{cmd})}{(\pi f T_{cmd})^2}\, df \qquad \text{NRZ} \qquad (36)$$

Equation (36) has no closed-form expression in terms of elementary functions. When the product $B_R T_{cmd} \ll 1$, $C_R(B_R T_{cmd}) \cong 2B_R T_{cmd}$. When $B_R T_{cmd} \gg 1$, $C_R(B_R T_{cmd}) \cong 1$. A general, approximate expression for $C_R(B_R T_{cmd})$ that is valid for high-rate command with NRZ pulses follows below. This approximation was obtained as a curve-fit of Equation (36) for intermediate values of the product $B_R T_{cmd}$.

$$C_R(B_R T_{cmd}) = \begin{cases} 2B_R T_{cmd}, & B_R T_{cmd} \leq 0.2 \\ \dfrac{1}{1 + \exp[-2.32 - 1.68 \cdot \ln(B_R T_{cmd})]}, & B_R T_{cmd} > 0.2 \end{cases} \qquad \text{NRZ} \qquad (37)$$

When high-rate command signaling consists of bi-phase (Manchester encoded) pulses that directly phase-modulate the uplink carrier, $C_R(B_R T_{cmd})$ may be modeled as

$$C_R(B_R T_{cmd}) = 2T_{cmd} \int_0^{B_R} \frac{\sin^4(\pi f T_{cmd}/2)}{(\pi f T_{cmd}/2)^2}\, df \qquad \text{bi-}\phi \qquad (38)$$

Equation (38) has no closed-form expression in terms of elementary functions. When the product $B_R T_{cmd} \ll 1$, $C_R(B_R T_{cmd}) \cong (\pi^2/6) \cdot (B_R T_{cmd})^3$. When $B_R T_{cmd} \gg 1$, $C_R(B_R T_{cmd}) \cong 1$. A general, approximate expression for $C_R(B_R T_{cmd})$ that is valid for high-rate command with bi-phase pulses follows below. This approximation was obtained as a curve-fit of Equation (38) for intermediate values of the product $B_R T_{cmd}$.

$$C_R(B_R T_{cmd}) = \begin{cases} \dfrac{\pi^2}{6} \cdot (B_R T_{cmd})^3, & B_R T_{cmd} \le 0.6 \\ \dfrac{1}{1 + \exp[-0.35 - 2.10 \cdot \ln(B_R T_{cmd})]}, & B_R T_{cmd} > 0.6 \end{cases} \quad \text{bi-}\phi \quad (39)$$

$C_R(B_R T_{cmd})$ is plotted as a function of $B_R T_{cmd}$ in Figure 4. This figure is for high-rate command that directly phase-modulates the uplink carrier. There is a curve for the case of NRZ pulses and second curve for the case of bi-phase pulses.

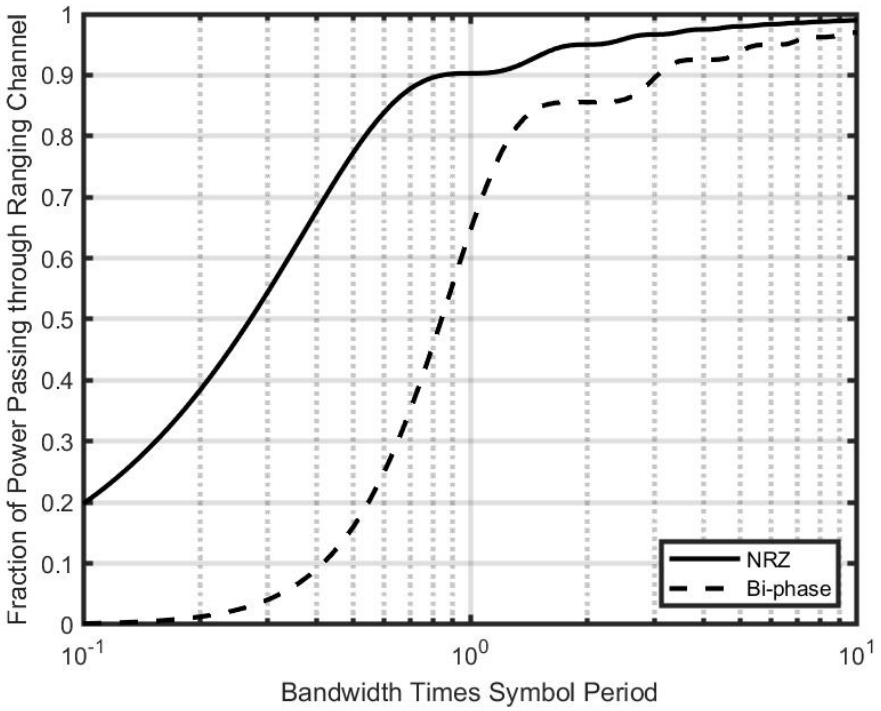

Figure 4. Fraction of Command Power Passing Ranging Channel

In some transponders with a turn-around ranging channel, the AGC is designed to keep constant the average of the absolute value of the voltage at the AGC output. In other transponders, the AGC is designed to keep constant the rms voltage at the AGC output. For both types of AGC, the downlink rms phase deviations θ_r, θ_n, and θ_{cmd} depend on ρ_r and ρ_{cmd} (as well as the parameter θ_{rs}). Turn-around ranging channels with both types of AGC are treated below.

2.3.2.1.1 AGC with Constant Average of Absolute Value of Voltage

When the transponder's ranging channel has an AGC that keeps constant the average of the absolute value of the channel voltage, there are no exact, analytical expressions for the rms phase deviations θ_r, θ_{cmd}, and θ_n. However, these rms phase deviations may be obtained by computer simulation. Curve fits to the simulations appear below.

$$\theta_r = \begin{cases} \theta_{rs} \cdot \dfrac{2\sqrt{2}}{\pi} \cdot \sqrt{\dfrac{\rho_r}{\rho_{cmd}}}, & \rho_{cmd} \geq 1 \text{ and } 0 < \rho_r \leq \rho_{cmd}/10 \\ \dfrac{\theta_{rs}}{1 + \exp[\gamma - 0.79 \cdot \ln(\rho_r)]}, & \text{otherwise} \end{cases} \tag{40}$$

where

$$\gamma = \begin{cases} -1.2, & \rho_{cmd} = 0 \\ \ln[0.3 + 0.27 \cdot {\rho_{cmd}}^{0.88}], & \rho_{cmd} > 0 \end{cases} \tag{41}$$

Here $\exp(\cdot)$ and $\ln(\cdot)$ are the exponential function and natural logarithm, respectively. In the event that there is no command feedthrough, $\rho_{cmd} = 0$ and θ_r depends only on the constant parameter θ_{rs} and the ranging signal-to-noise ratio ρ_r. The asymptotes for Equation (40) are $\lim_{\rho_r \to 0} \theta_r = 0$ and $\lim_{\rho_r \to \infty} \theta_r = \theta_{rs}$.

A similar set of equations are valid (approximately) for θ_{cmd}

$$\theta_{cmd} = \frac{\theta_{rs}}{1 + \exp[\chi - 0.79 \cdot \ln(\rho_{cmd})]} \tag{42}$$

where

$$\chi = \ln[0.3 + 0.27 \cdot {\rho_r}^{0.88}] \tag{43}$$

The asymptotes for Equation (42) are $\lim_{\rho_{cmd} \to 0} \theta_{cmd} = 0$ and $\lim_{\rho_{cmd} \to \infty} \theta_{cmd} = \theta_{rs}$.

A curve-fit to the simulation data for θ_n as a function of ρ_r and ρ_{cmd} is:

$$\theta_n = \frac{\theta_{rs} \cdot \left(2/\sqrt{\pi}\right)}{1 + \exp[-0.87 + 0.81 \cdot \ln(\rho_{rss})]} \tag{44}$$

where ρ_{rss} is the root-sum-square of ρ_r and ρ_{cmd}:

$$\rho_{rss} = \sqrt{{\rho_r}^2 + {\rho_{cmd}}^2} \tag{45}$$

The asymptotes for this curve are $\lim_{\rho_{rss} \to 0} \theta_n = \theta_{rs} \cdot \left(2/\sqrt{\pi}\right)$ and $\lim_{\rho_{rss} \to \infty} \theta_n = 0$.

Since θ_r is directly proportional to the parameter θ_{rs}, the ratio θ_r/θ_{rs} may be plotted as a function of ρ_r (and ρ_r alone when $\rho_{cmd} = 0$). This appears in Figure 5 for the case of no command feedthrough: $\rho_{cmd} = 0$ and $\theta_{cmd} = 0$. The solid curve labeled AAV is valid for a turn-around ranging channel whose AGC keeps constant the average of the absolute voltage (AAV). Figure 5 shows that the ratio θ_r/θ_{rs} increases monotonically as a function of ρ_r with a limiting value of 1. (In other words, the strong-signal value of θ_r is θ_{rs}.) The AAV curve of Figure 5 comes from Equations (40) and (41) with $\rho_{cmd} = 0$.

The ratio θ_n/θ_{rs} may also be plotted as a function of ρ_r when $\rho_{cmd} = 0$. This appears in Figure 6. The solid curve labeled AAV is valid for a turn-around ranging channel whose AGC keeps constant the average of the absolute voltage (AAV). Figure 6 shows that the ratio θ_n/θ_{rs} decreases monotonically as a function of ρ_r. The AAV curve of Figure 6 comes from Equations (44) and (45) with $\rho_{cmd} = 0$.

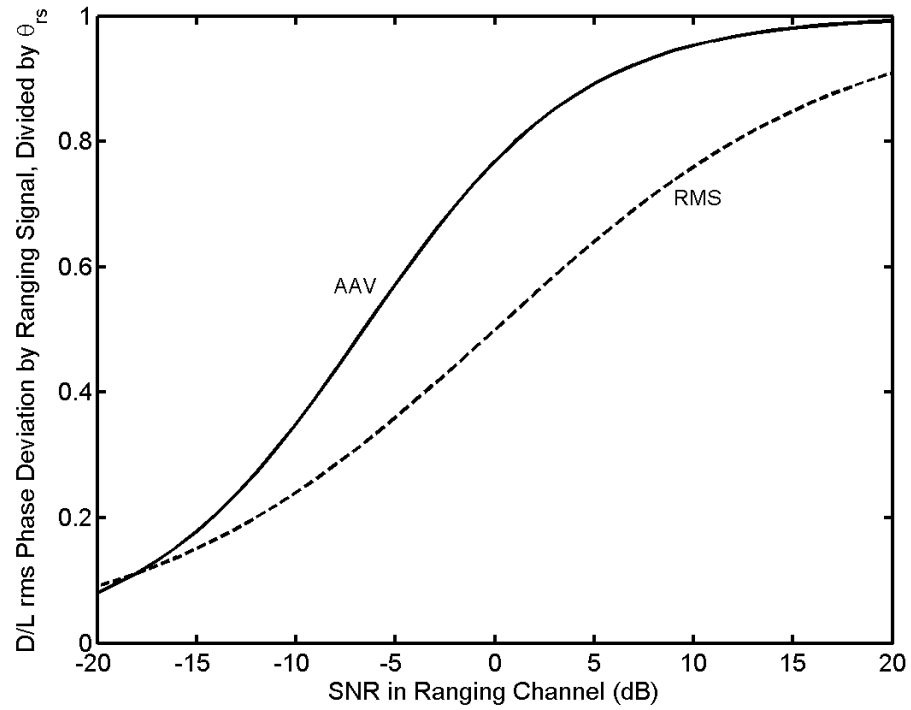

Figure 5. Downlink rms Phase Deviation by Ranging Signal (No Command Feedthrough)

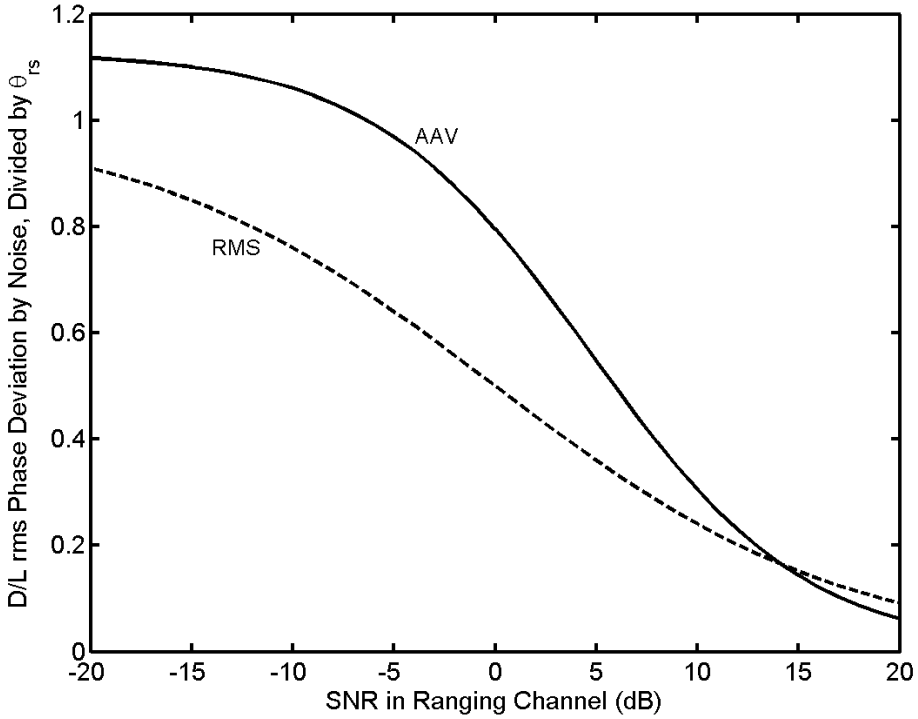

Figure 6. Downlink rms Phase Deviation by Noise (No Command Feedthrough)

2.3.2.1.2 AGC with Constant Root-Mean-Square Voltage

In some transponders, especially older designs, the ranging channel has an AGC that enforces a constant rms voltage at the AGC output. Since an unchanging rms voltage corresponds to an unchanging power, this type of AGC is also called a power-controlled AGC.

An AGC that enforces constant rms voltage (equivalently, constant power) at the AGC output is characterized by the following relationship among the rms phase deviations θ_r, θ_{cmd}, θ_n, and θ_{rs}.

$$\theta_r{}^2 + \theta_{cmd}{}^2 + \theta_n{}^2 = \theta_{rs}{}^2 \tag{46}$$

In other words, the total power in the turn-around ranging channel, which equals the ranging signal power plus the feedthrough command signal power plus the noise power in the channel bandwidth, equals a constant value. The rms phase deviations are given by

$$\theta_r = \theta_{rs} \cdot \sqrt{\frac{\rho_r}{1 + \rho_r + \rho_{cmd}}} \tag{47}$$

$$\theta_{cmd} = \theta_{rs} \cdot \sqrt{\frac{\rho_{cmd}}{1 + \rho_r + \rho_{cmd}}} \tag{48}$$

$$\theta_n = \frac{\theta_{rs}}{\sqrt{1 + \rho_r + \rho_{cmd}}} \tag{49}$$

The ratio θ_r/θ_{rs} is plotted as a function of ρ_r in Figure 5 for the case of no command feedthrough: $\rho_{cmd} = 0$ and $\theta_{cmd} = 0$. The dashed curve labeled RMS is valid for a turn-around ranging channel whose AGC enforces a constant rms voltage at the AGC output. The RMS curve of Figure 5 comes from Equation (47) with $\rho_{cmd} = 0$.

The ratio θ_n/θ_{rs} is plotted as a function of ρ_r in Figure 6 for the case of no command feedthrough: $\rho_{cmd} = 0$ and $\theta_{cmd} = 0$. The dashed curve labeled RMS is valid for a turn-around ranging channel whose AGC enforces a constant rms voltage at the AGC output. The RMS curve of Figure 6 comes from Equation (49) with $\rho_{cmd} = 0$.

2.3.2.1.3 Comparison of Two AGC Types

As explained above, there are two types of AGC that have been employed in transponders with turn-around ranging channels. These two AGCs differ in the quantity that is kept constant: either the average of the absolute voltage (AAV) or the root-mean-square (RMS).

Figure 7 plots $P_R/P_T|_{D/L}$ as a function of ρ_r for each of the two AGC types. For all curves in this figure, there is no telemetry and there is no command feedthrough. For each AGC type, there are two curves: one for $\theta_{rs} = 0.2$ rad rms and a second for $\theta_{rs} = 0.4$ rad rms. $P_R/P_T|_{D/L}$ was calculated using Equation (27). The phase deviations θ_r and θ_n needed within

Equation (27) were calculated using the equations of Subsection 2.3.2.1.1 for the AAV curves and Subsection 2.3.2.1.2 for the RMS curves.

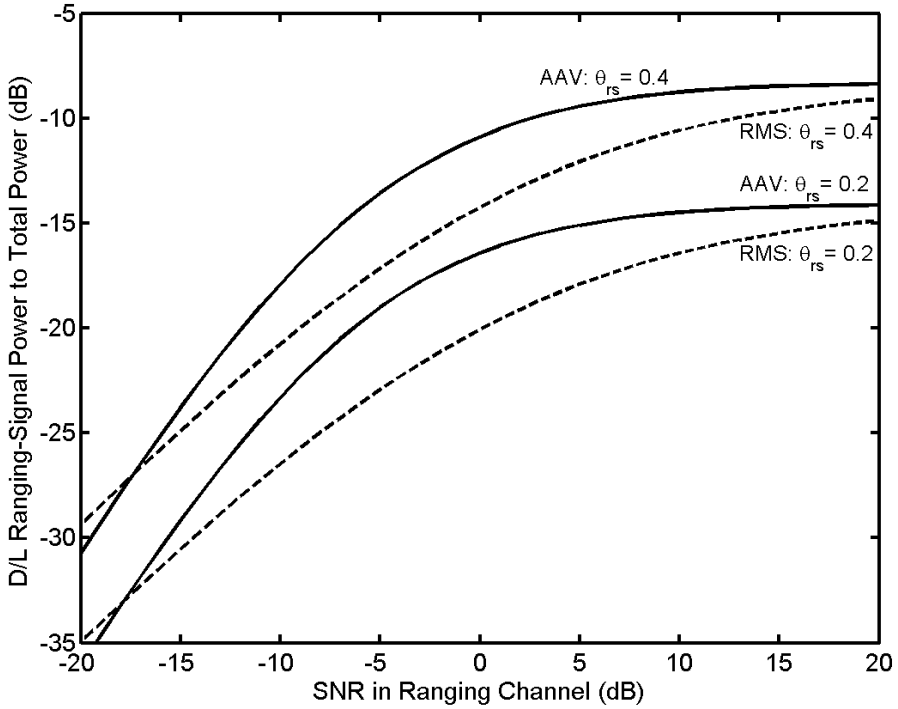

Figure 7. Downlink Ranging-Signal Power to Total Power (No Telemetry, No Command)

Figure 8 plots the carrier suppression $P_C/P_T|_{D/L}$ as a function of ρ_r for each of the two AGC types. For all curves in this figure, there is no telemetry and there is no command feedthrough. For each AGC type, there are two curves: one for $\theta_{rs} = 0.2$ rad rms and a second for $\theta_{rs} = 0.4$ rad rms. $P_C/P_T|_{D/L}$ was calculated using Equation (26). The phase deviations θ_r and θ_n needed within Equation (26) were calculated using the equations of Subsection 2.3.2.1.1 for the AAV curves and Subsection 2.3.2.1.2 for the RMS curves.

2.3.2.2 Regenerative Ranging

A regenerative ranging channel demodulates the uplink carrier, tracks the range clock, detects the range code, and modulates a ranging signal on the downlink. A regenerative ranging channel produces a clean ranging signal, free of command feedthrough and with little noise, because this channel has a small bandwidth. (This bandwidth is orders-of-magnitude smaller than the 1.5-MHz bandwidth of the typical turn-around ranging channel.)

A transponder that supports regenerative ranging will, of necessity, be designed to track a specific PN range code. This could be the DSN range code, the T4B range code, or the T2B range code. The equations appearing in this subsection are applicable to any of these three PN range codes, as long as the transponder in question is designed to support regenerative ranging with that particular range code.

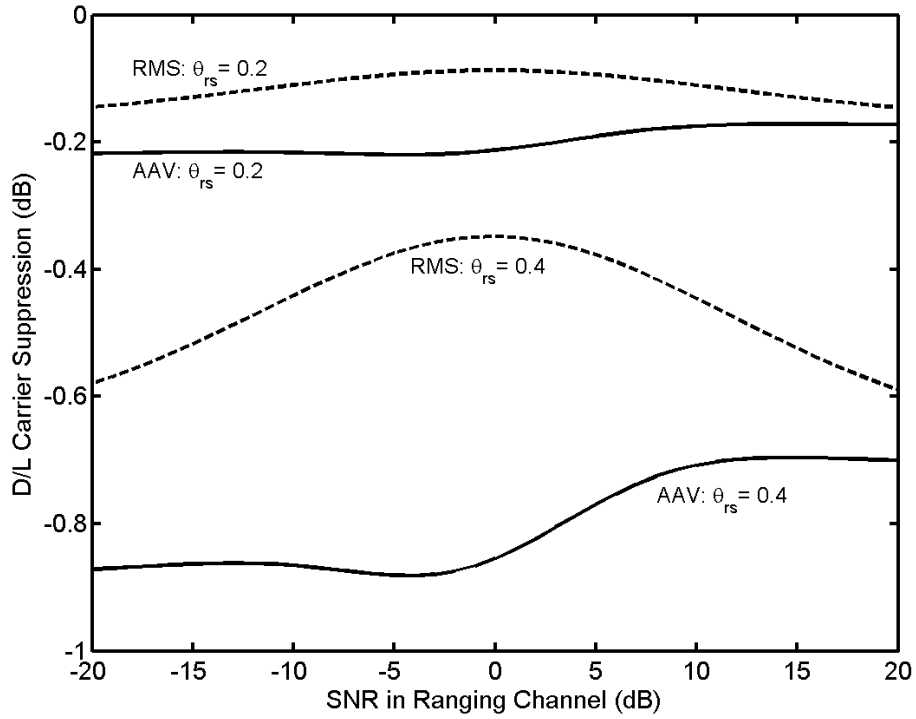

Figure 8. Downlink Carrier Suppression (No Telemetry, No Command)

For the purpose of calculating the distribution of power on the downlink in the case of regenerative ranging, the following equations may be used. There will, in general, be phase jitter on the downlink ranging signal that is caused by uplink thermal noise and this jitter is an error source for the two-way range measurement. This error is considered in Section 2.5.

The carrier suppression is

$$\left.\frac{P_C}{P_T}\right|_{\mathrm{D/L}} = {J_0}^2\left(\sqrt{2}\,\theta_{rs}\right)\cdot\cos^2(\theta_{tlm}) \tag{50}$$

The ratio of available ranging signal power to total power is

$$\left.\frac{P_R}{P_T}\right|_{\mathrm{D/L}} = 2\,{J_1}^2\left(\sqrt{2}\,\theta_{rs}\right)\cdot\cos^2(\theta_{tlm}) \tag{51}$$

The ratio of available telemetry (data) signal power to total power is

$$\left.\frac{P_D}{P_T}\right|_{\mathrm{D/L}} = {J_0}^2\left(\sqrt{2}\,\theta_{rs}\right)\cdot\sin^2(\theta_{tlm}) \tag{52}$$

In these equations, θ_{rs} is the (strong-signal) rms phase deviation of the downlink carrier by the ranging signal, and θ_{tlm} is the telemetry modulation index.

2.4 Uplink Spectrum

The spectrum of the uplink carrier is of some concern because of the very large transmitter powers used on the uplink for deep space missions. A mathematical model for this spectrum is given here for the case of a sinewave range clock and no command.

A PN ranging signal is periodic, so its spectrum consists of discrete spectral lines. The spectrum of an uplink carrier that has been phase modulated by only a PN ranging signal also consists of discrete spectral lines.

As described in Section 2.2, the composite chip sequence $c'(\cdot)$ is similar to the range clock $c_1{}'(\cdot)$, except that some chips are inverted. A discrepancy signal $d'(\cdot)$ is defined by

$$d'(i) = c_1{}'(i) \cdot c'(i) \tag{53}$$

$d'(i)$ equals $+1$ when the range clock and the composite code agree, which is most of the time. When the range clock and the composite code disagree, $d'(i)$ equals -1. The PN ranging signal may be mathematically modeled as $d(i)\sin(\pi t/T_c)$ for $iT_c \le t < (i+1)T_c$, where T_c is the chip period. In words, the PN ranging signal is a sinewave (range clock) of frequency $1/(2T_c)$ except that there is an occasional inversion of a half-cycle. When this signal phase modulates the uplink carrier with an rms phase deviation ϕ_r (radians rms), the fractional power in each discrete spectral line is given by

$$\frac{P_k}{P_T} = |X_k|^2 = \begin{cases} \text{fraction of uplink total power in the} \\ \text{discrete spectral line with frequency} \\ f_C + \dfrac{k}{LT_c} \end{cases} \tag{54}$$

where P_T is the total uplink power, f_C is the uplink carrier frequency, L is the period in chips of the composite code, k is an integer harmonic number, and X_k is given by

$$X_k = \frac{1}{L}\sum_{m=-\infty}^{\infty} \operatorname{sinc}\left(\frac{m}{2} - \frac{k}{L}\right) \sum_{n=0}^{L-1} J_m\left(\sqrt{2}\,\phi_r\, d'(n)\right) \exp\left[j\pi\left(n+\frac{1}{2}\right)\left(m - \frac{2k}{L}\right)\right] \tag{55}$$

where $J_m(\cdot)$ is the Bessel function of the first kind of order m, and

$$\operatorname{sinc}(x) = \frac{\sin(\pi x)}{\pi x} \tag{56}$$

Equation (55) may be evaluated numerically. The values of the Bessel functions decrease very rapidly with increasing $|m|$, so in practice it is possible to get good accuracy while including only a few terms from the sum over the integer m. In evaluating Equation (55), the following identity is useful.

$$J_{-m}(x) = \begin{cases} J_m(x), & m \text{ even} \\ -J_m(x), & m \text{ odd} \end{cases} \tag{57}$$

There is a symmetrical power distribution about the carrier. So for every discrete spectral line at $f_C + k/(LT)$ whose power is given by Equation (54), there is also a discrete spectral line at $f_C - k/(LT)$ with the same power.

Figure 9 illustrates the uplink spectrum for a sinewave range clock with the DSN range code and an rms phase deviation $\phi_r = 0.2$ rad rms. The horizontal axis represents the ratio of the frequency offset from the residual carrier to the range-clock frequency. The vertical axis is the ratio of the power in a discrete-spectral line to the total signal power, expressed in decibels. The residual carrier is located at the horizontal coordinate 0, and it has a power of -0.2 dB relative to P_T. In other words, the carrier suppression is -0.2 dB. The lower fundamental harmonic has a horizontal coordinate of -1 (a frequency of $f_C - f_{RC}$), and the upper fundamental harmonic has a horizontal coordinate of $+1$ (a frequency of $f_C + f_{RC}$); each of these has a power of -17.5 dB relative to P_T. The lower second harmonic has a horizontal coordinate of -2 (a frequency of $f_C - 2f_{RC}$), and the upper second harmonic has a horizontal coordinate of $+2$ (a frequency of $f_C + 2f_{RC}$); each of these has a power of -39.7 dB relative to P_T. The smaller spectral lines that lie between $f_C - 2f_{RC}$ and $f_C + 2f_{RC}$ arise from the occasional inversions of half-cycles as represented by $d'(i)$; this is the spectrum spreading that permits the amibiguity to be resolved.

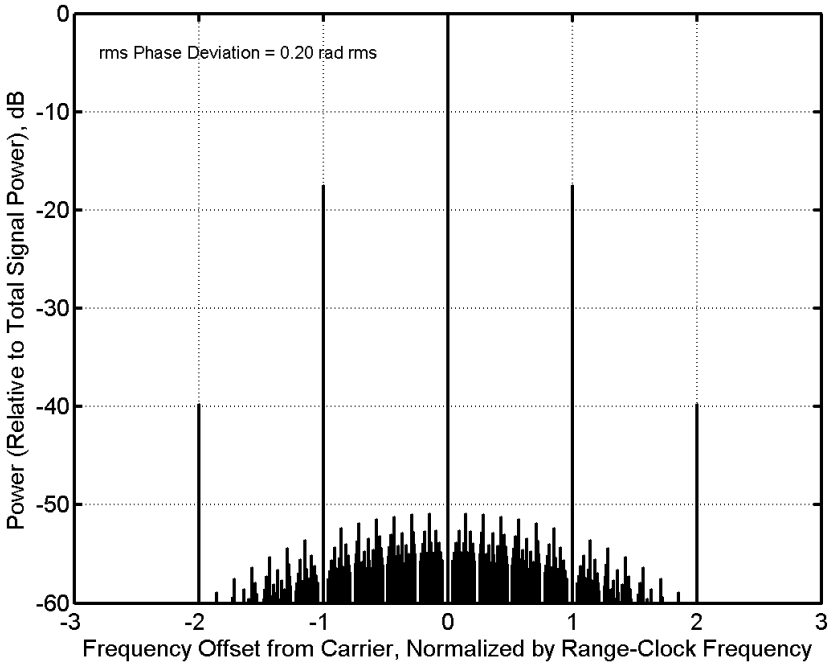

Figure 9. Uplink Spectrum for the DSN Range Code Ranging Signal

2.5 Range Measurement Performance

Thermal noise has two effects on range measurements. First, there is a standard deviation of range measurement error due to thermal noise. Second, there is a probability of acquisition of the range measurement that is less than 100% due to the presence of thermal noise. The cross-correlation factors of a composite code plays a role in the performance of PN ranging in the presence of thermal noise.

2.5.1 Cross-Correlation Factors

The cross-correlation factors R_n (with zero delay) are defined by

$$R_n = \frac{1}{L}\sum_{i=0}^{L-1} c'(i)c_n{}'(i) \tag{58}$$

where L is the period (in chips) of the composite code, $c'(i) = \pm 1$ is the chip sequence, and $c_n{}'(i) = \pm 1$ is the (periodic extension of the) chip sequence for the n-th component code. The cross-correlation factors are given in tables that follow: Table 3 for the DSN range code, Table 4 for the T4B code, and Table 5 for the T2B code.

Table 3. Cross-Correlation Factors, DSN Range Code

n	λ_n	R_n
1	2	0.9544
2	7	0.0456
3	11	0.0456
4	15	0.0456
5	19	0.0456
6	23	0.0456

Table **4**. Cross-Correlation Factors, T4B (Reference 4)

n	λ_n	R_n
1	2	0.9387
2	7	0.0613
3	11	0.0613
4	15	0.0613
5	19	0.0613
6	23	0.0613

Table 5. Cross-Correlation Factors, T2B (Reference 4)

n	λ_n	R_n
1	2	0.6274
2	7	0.2447
3	11	0.2481
4	15	0.2490
5	19	0.2492
6	23	0.2496

2.5.2 Downlink Ranging Signal Power to Noise Spectral Density

P_R/N_0, the ratio of the downlink ranging signal power to noise spectral density, is given by

$$\frac{P_R}{N_0} = \frac{P_R}{P_T}\Big|_{\mathrm{D/L}} \cdot \frac{P_T}{N_0}\Big|_{\mathrm{D/L}} \tag{59}$$

Equation (59) is applicable when there are no significant sources of interference (beyond the downlink thermal noise). Considered in the next subsection is the scenario where additional interference is present. $P_T/N_0|_{D/L}$ is the downlink total signal to noise spectral density ratio. $P_R/P_T|_{D/L}$ is the ratio of downlink ranging signal power to total power. $P_R/P_T|_{D/L}$ is given by Equation (27) for turn-around (non-regenerative) ranging and by Equation (51) for regenerative ranging.

2.5.3 Effect of Interference

In addition to the thermal noise that arises on the downlink, which is characterized by the noise spectral density $N_0|_{\mathrm{D/L}}$, there are sources of interference to the range measurement. Often the most important interference to the range measurement is telemetry; this interference occurs when there is spectral overlap of telemetry sidebands with the PN code components. When a non-regenerative (turn-around) ranging channel is used, the uplink noise and command signal can pass through the ranging channel and become modulated onto the downlink carrier. Finally, there are intermodulation products on the downlink.

In quantifying the effect of interference on range measurement, one considers the quadrature channel of the downlink receiver. It is in this quadrature receiver channel that the range correlations occur. The model employed here regards the interference in the quadrature channel as folding into the downlink thermal noise, so that the *effective* downlink noise spectral density is $N_0|_{\mathrm{D/L}} \cdot \Gamma_Q$, where $\Gamma_Q \geq 1$. In other words, Γ_Q is the factor by which the downlink noise floor increases in the downlink receiver's quadrature channel due to the presence of

telemetry, command feedthrough, uplink noise (that has been transponded to the downlink), and intermodulation products. This is the model used in Reference 3.

Another, equivalent way of stating the above is to define an effective P_R/N_0.

$$\text{effective } \frac{P_R}{N_0} = \frac{P_R}{P_T}\bigg|_{\mathrm{D/L}} \cdot \frac{P_T}{N_0}\bigg|_{\mathrm{D/L}} \cdot \frac{1}{\Gamma_Q} \tag{60}$$

When significant interference is present, the effective P_R/N_0 is smaller than that given by Equation (59). In this case, the effective P_R/N_0 should be calculated from Equation (60).

The various sources of interference in the quadrature channel may be taken into account in this manner:

$$\Gamma_Q = 1 + \mathrm{K}_{NQ} + \mathrm{K}_{tlm} + \mathrm{K}_{fth} \tag{61}$$

where

K_{NQ} = contribution from intermodulation products and transponded uplink noise
K_{tlm} = contribution from telemetry
K_{fth} = contribution from feedthrough command

For a non-regenerative ranging channel, K_{NQ} may be approximated as

$$\mathrm{K}_{NQ} = \frac{1}{B_R} \cdot \frac{P_T}{N_0}\bigg|_{\mathrm{D/L}} \cdot \frac{P_{NQ}}{P_T}\bigg|_{\mathrm{D/L}} \tag{62}$$

where $P_T/N_0|_{D/L}$ is the downlink total signal to noise spectral density ratio and B_R is the bandwidth of the transponder's ranging channel. The new term $P_{NQ}/P_T\big|_{D/L}$ is the power in uplink noise (transponded to the downlink) and quadrature-channel intermodulation products, relative to the total downlink power.

$$\begin{aligned} \frac{P_{NQ}}{P_T}\bigg|_{\mathrm{D/L}} &= {\theta_n}^2 \\ &\cdot e^{-{\theta_n}^2} \\ &\times \left[{J_0}^2\left(\sqrt{2}\,\theta_r\right) \cdot \cos^2(\theta_{cmd}) \cdot \cos^2(\theta_{tlm})\right. \\ &+ 2{J_1}^2\left(\sqrt{2}\,\theta_r\right) \cdot \cos^2(\theta_{cmd}) \cdot \sin^2(\theta_{tlm}) \\ &\left.+ {J_0}^2\left(\sqrt{2}\,\theta_r\right) \cdot \sin^2(\theta_{cmd}) \cdot \sin^2(\theta_{tlm})\right] \end{aligned} \tag{63}$$

The variables θ_r, θ_{tlm}, θ_{cmd}, and θ_n have been defined previously. They are the rms phase deviations of the downlink carrier due to a ranging signal (θ_r), telemetry (θ_{tlm}), command feedthrough (θ_{cmd}), and transponded uplink noise (θ_n).

The following subsections provide models for K_{tlm} and K_{fth} that are applicable to bi-polar telemetry and bi-polar command. As before, "bi-polar" means either NRZ or bi-phase pulses that directly phase-modulate the carrier. These models for K_{tlm} and K_{fth}, in their most general form, are complicated. Therefore, curve-fit approximations are also given below; these curve-fit approximations should ease the task of implementing interference models in a spreadsheet.

2.5.3.1 Interference from Telemetry and Feedthrough Command (Bi-Polar Signaling)

The models for K_{tlm} and K_{fth} given here are applicable to bi-polar telemetry and bi-polar command. In other words, it is assumed here that NRZ or bi-phase symbols directly phase-modulate the carrier.

For each PN code component, the effect of the interference on that component's correlation is calculated. ${K^{(n)}}_{tlm}$ characterizes the telemetry interference to the correlation of component n, for $n = 1, 2, 3, 4, 5,$ or 6. Similarly, ${K^{(n)}}_{fth}$ characterizes the feedthrough-command interference to the correlation of component n. The six PN code components are listed in Table 2. All three of the range codes—DSN, T4B, and T2B—are built from this common set of PN code components. (The differences among the DSN, T4B, and T2B range codes arise from how the PN code components are combined.) Because the models given below are based on the correlations with the 6 PN code components and because these PN code components are the same for all three range codes—DSN, T4B, and T2B—these models are applicable to all three range codes.

K_{tlm} is taken to be the maximum of the six ${K^{(n)}}_{tlm}$, $n = 1, 2, 3, 4, 5,$ or 6.

$$\mathrm{K}_{tlm} = \max_{n} {K^{(n)}}_{tlm} \tag{64}$$

Equation (64) is an approximation; it is based on the idea that the weakest correlation defines, approximately, the performance of the range measurement in the presence of thermal noise plus telemetry interference.

In the model for the effect of command feedthrough, K_{fth} is taken to be the maximum of the six ${K^{(n)}}_{fth}$, $n = 1, 2, 3, 4, 5,$ or 6.

$$\mathrm{K}_{fth} = \max_{n} {K^{(n)}}_{fth} \tag{65}$$

Equation (65) is an approximation; it is based on the idea that the weakest correlation defines, approximately, the performance of the range measurement in the presence of thermal noise plus command-feedthrough interference.

The individual ${K^{(n)}}_{tlm}$ are calculated as

$${K^{(n)}}_{tlm} = \left.\frac{P_T}{N_0}\right|_{\mathrm{D/L}} \cdot \left.\frac{P_D}{P_T}\right|_{\mathrm{D/L}} \cdot \begin{cases} S_{tlm}(f_{1,1}), & n = 1 \\ \sum_{k=0}^{\infty} P_{n,k}\, S_{tlm}(f_{n,k}), & 2 \le n \le 6 \end{cases} \tag{66}$$

$P_T/N_0|_{D/L}$ is the downlink total signal to noise spectral density ratio. $P_D/P_T|_{D/L}$ is the ratio of telemetry power to total power, as given by Equation (28). $S_{tlm}(\cdot)$ is the one-sided, unity-power, power spectral density of telemetry, an expression for which appears below. The variables $f_{n,k}$ and $P_{n,k}$ are the frequencies and relative powers of discrete spectral lines associated with component PN code n.

The individual ${K^{(n)}}_{fth}$ are calculated as

$$K^{(n)}{}_{fth} = \left.\frac{P_T}{N_0}\right|_{\mathrm{D/L}} \cdot \left.\frac{P_{fth}}{P_T}\right|_{\mathrm{D/L}} \cdot \begin{cases} S_{cmd}(f_{1,1}), & n = 1 \\ \sum_{k=0}^{\infty} P_{n,k}\, S_{cmd}(f_{n,k}), & 2 \le n \le 6 \end{cases} \tag{67}$$

$\left.P_{fth}/P_T\right|_{D/L}$ is the ratio of feedthrough-command power to total power, which is given by Equation (29). $S_{cmd}(\cdot)$ is the one-sided, unity-power, power spectral density of command, an expression for which appears below. The variables $f_{n,k}$ and $P_{n,k}$ are the frequencies and relative powers of discrete spectral lines associated with component PN code n.

The one-sided, unity-power, power spectral density of telemetry is

$$S_{tlm}(f) = \begin{cases} 2T_{tlm} \cdot \dfrac{\sin^2(\pi f T_{tlm})}{(\pi f T_{tlm})^2}, & \mathrm{NRZ} \\ 2T_{tlm} \cdot \dfrac{\sin^4(\pi f T_{tlm}/2)}{(\pi f T_{tlm}/2)^2}, & \mathrm{Bi-phase} \end{cases} \tag{68}$$

where T_{tlm} is the telemetry symbol period.

The one-sided, unity-power, power spectral density of command is

$$S_{cmd}(f) = \begin{cases} 2T_{cmd} \cdot \dfrac{\sin^2(\pi f T_{cmd})}{(\pi f T_{cmd})^2}, & \mathrm{NRZ} \\ 2T_{cmd} \cdot \dfrac{\sin^4(\pi f T_{cmd}/2)}{(\pi f T_{cmd}/2)^2}, & \mathrm{Bi-phase} \end{cases} \tag{69}$$

where T_{cmd} is the command symbol period.

Each PN code component $c_n{}'$ has a period of λ_n. The spectrum of $c_n{}'$ consists of discrete spectral lines. The k-th spectral line of $c_n{}'$ is denoted here by the ordered pair (n, k). The frequency of the (n, k) spectral line is denoted $f_{n,k}$. For example, the (1, 1) spectral line is the fundamental ($k = 1$) harmonic of the first code component; in other words, $f_{1,1}$ is the range-clock frequency. The general expression for $f_{n,k}$ is

$$f_{n,k} = \frac{k f_{\mathrm{chip}}}{\lambda_n} \qquad \begin{matrix} k \ge 0 \\ 2 \le n \le 6 \end{matrix} \tag{70}$$

where f_{chip} is the chip rate of the range code. The discrete Fourier transform (DFT) $\tilde{C}_n(k)$ of each $c_n{}'$ is required. The DFT of $c_n{}'$ is calculated using λ_n samples. The fractional power $P_{n,k}$ in the discrete spectral line at frequency $f_{n,k}$ is given by

$$P_{n,k} = 2 \cdot \frac{\sin^2(\pi k/\lambda_n)}{(\pi k)^2} \cdot \left|\tilde{C}_n(k)\right|^2 \qquad \begin{matrix} k \ge 0 \\ 2 \le n \le 6 \end{matrix} \tag{71}$$

The equations of this subsection permit calculation of K_{tlm} and K_{fth}. The only $S_{tlm}(f)$ and $S_{cmd}(f)$ models provided here are for the cases of NRZ or bi-phase pulses directly phase-modulated on the carrier.

2.5.3.2 Curve-Fit Approximations for Interference Models

The interference models of Subsection 2.5.3.1 are approximate models, but even those approximate models are rather complicated. Curve-fits to those models are given below. Of course, the curve-fits represent an additional layer of approximation.

The curve-fit for the telemetry interference model is accomplished by first rewriting Equations (64) and (66) as

$$\mathrm{K}_{tlm} = \left.\frac{P_T}{N_0}\right|_{\mathrm{D/L}} \cdot \left.\frac{P_D}{P_T}\right|_{\mathrm{D/L}} \cdot T_{tlm} \cdot \hat{S}_{tlm}(f_{\mathrm{chip}} T_{tlm}) \tag{72}$$

where

$$\hat{S}_{tlm}(f_{\mathrm{chip}} T_{tlm}) = \frac{1}{T_{tlm}} \cdot \max_n \begin{cases} S_{tlm}(f_{1,1}), & n = 1 \\ \sum_{k=0}^{\infty} P_{n,k}\, S_{tlm}(f_{n,k}), & 2 \le n \le 6 \end{cases} \tag{73}$$

$\hat{S}_{tlm}(f_{\mathrm{chip}} T_{tlm})$ is the maximum (over the six PN code components) of the weighted average of the one-sided, unity-power, telemetry power spectral density, normalized by the telemetry symbol period. The weighted average occurs over the frequencies ($f_{n,k}$) associated with the discrete spectral lines of each PN code component.

$\hat{S}_{tlm}(f_{\mathrm{chip}} T_{tlm})$ is a function of the product of the chip rate f_{chip} and the telemetry symbol period T_{tlm}. Both the input $f_{\mathrm{chip}} T_{tlm}$ and the output of the function $\hat{S}_{tlm}(f_{\mathrm{chip}} T_{tlm})$ are dimensionless. $\hat{S}_{tlm}(f_{\mathrm{chip}} T_{tlm})$ also depends on the nature of the telemetry spectrum. A curve-fit appears below both for NRZ telemetry symbols and for bi-phase telemetry symbols (directly phase-modulating the downlink carrier). For NRZ telemetry,

$$\hat{S}_{tlm}(f_{\mathrm{chip}} T_{tlm}) \cong 0.090 + 1.88 \exp(-0.46\, f_{\mathrm{chip}} T_{tlm}) \qquad \text{NRZ} \tag{74}$$

For bi-phase telemetry,

$$\hat{S}_{tlm}(f_{\mathrm{chip}} T_{tlm}) \cong \begin{cases} 2 \cdot \sin^4(\pi f_{\mathrm{chip}} T_{tlm}/4)/(\pi f_{\mathrm{chip}} T_{tlm}/4)^2, & f_{\mathrm{chip}} T_{tlm} \le 2.25 \\ 0.090 + 0.77 \exp(-0.20\, f_{\mathrm{chip}} T_{tlm}), & f_{\mathrm{chip}} T_{tlm} > 2.25 \end{cases} \tag{75}$$

Equation (72) can also be written as

$$\mathrm{K}_{tlm} = \left.\frac{E_S}{N_0}\right|_{\mathrm{D/L}} \cdot \hat{S}_{tlm}(f_{\mathrm{chip}} T_{tlm}) \tag{76}$$

where $E_S/N_0|_{\mathrm{D/L}}$ is the ratio of the telemetry symbol energy to the noise spectral density, and where this noise spectral density only accounts for thermal noise originating on the downlink.

$\hat{S}_{tlm}(f_{\mathrm{chip}} T_{tlm})$ is plotted as a function of $f_{\mathrm{chip}} T_{tlm}$ for both NRZ telemetry and for bi-phase telemetry in Figure 10. For the bi-phase curve, there is a slope discontinuity at $f_{\mathrm{chip}} T_{tlm} = 2.25$. This slope discontinuity originates with the approximation of Equation (64).

For $f_{\text{chip}}T_{tlm} \leq 2.25$, the largest term is that associated with the range clock; this dominant term is $K^{(1)}{}_{tlm}$. For $f_{\text{chip}}T_{tlm} > 2.25$, the largest term is one of the others: $K^{(n)}{}_{tlm}$ for $2 \leq n \leq 6$.

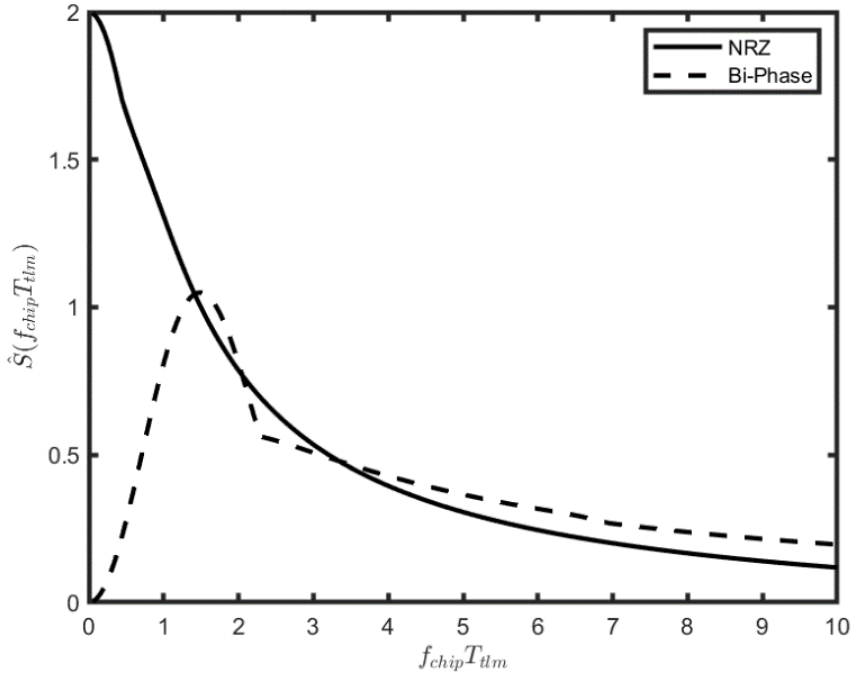

Figure 10. Curve-Fit Function for Modeling Increase in Quadrature-Channel Noise Floor

Once $\hat{S}_{tlm}(f_{\text{chip}}T_{tlm})$ is determined from a curve-fit, Equation (72) or (76) can be used to calculate K_{tlm}. In general, there can be other sources of interference (in addition to telemetry) that must be taken into account. Equation (61) is used to calculate Γ_Q.

Figure 11 plots Γ_Q, in decibels, as a function of $f_{\text{chip}}T_{tlm}$ with $E_S/N_0|_{\text{D/L}}$ as a parameter. This figure represents a scenario where telemetry is the only source of interference to the range measurement and the telemetry symbols are NRZ. The three curves in this figure correspond to the following values of $E_S/N_0|_{\text{D/L}}$: -3 dB, 0 dB, and $+3$ dB. The larger the $E_S/N_0|_{\text{D/L}}$, the larger is Γ_Q. Also, for NRZ telemetry, Γ_Q becomes larger as $f_{\text{chip}}T_{tlm}$ decreases.

The upper bound on K_{tlm} for NRZ telemetry is

$$\text{K}_{tlm} \leq 2T_{tlm} \cdot \frac{P_T}{N_0}\bigg|_{\text{D/L}} \cdot \frac{P_D}{P_T}\bigg|_{\text{D/L}} \qquad \text{NRZ} \qquad (77)$$

$P_T/N_0|_{D/L}$ is the downlink total signal to noise spectral density ratio. $P_D/P_T|_{D/L}$ is the ratio of telemetry power to total power, as given by Equation (28). When the telemetry symbol rate is large compared with the range-code chip rate (that is, when $f_{\text{chip}}T_{tlm} \ll 1$), this upper bound on K_{tlm} for NRZ telemetry is tight and the upper bound is a good approximation for K_{tlm}.

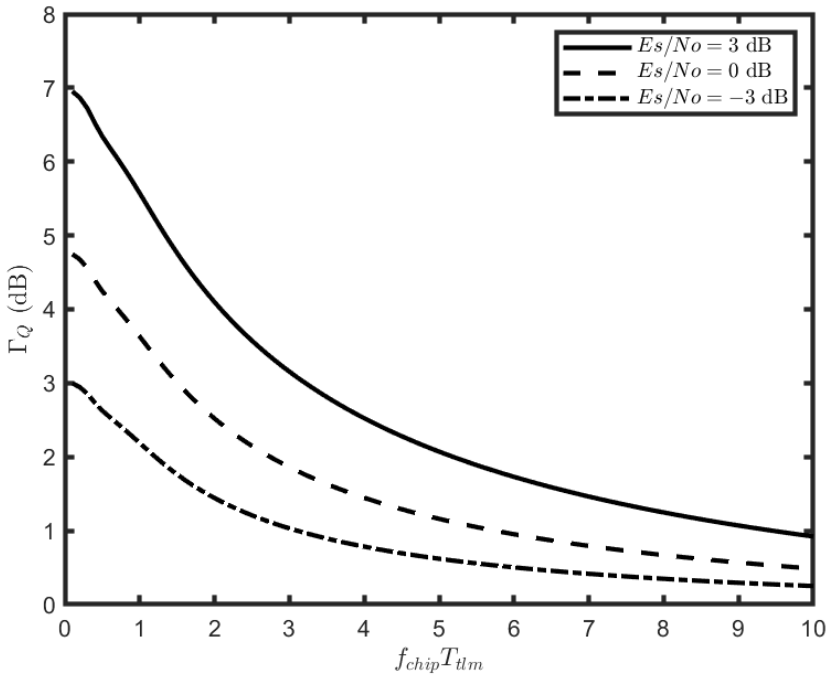

Figure 11. Increase (dB) in Range-Measurement Noise Floor Due to NRZ Telemetry

The upper bound on K_{tlm} for bi-phase telemetry is

$$\mathrm{K}_{tlm} \leq 1.1 \cdot T_{tlm} \cdot \frac{P_T}{N_0}\Big|_{\mathrm{D/L}} \cdot \frac{P_D}{P_T}\Big|_{\mathrm{D/L}} \qquad \text{bi-phase} \qquad (78)$$

For bi-phase telemetry when $f_{\mathrm{chip}}T_{tlm} \ll 1$, the telemetry interference to a range measurement may be negligible.

The procedure for calculating K_{fth}, which is needed to estimate the effect of command-feedthrough interference on the range measurement, is very similar to the calculation of K_{tlm}. In order to take advantage of curve-fits, K_{fth} can be calculated by

$$\mathrm{K}_{fth} = \frac{P_T}{N_0}\Big|_{\mathrm{D/L}} \cdot \frac{P_{fth}}{P_T}\Big|_{\mathrm{D/L}} \cdot T_{cmd} \cdot \hat{S}_{cmd}(f_{\mathrm{chip}}T_{cmd}) \qquad (79)$$

where $P_T/N_0|_{D/L}$ is the downlink total signal to noise spectral density ratio and $P_{fth}/P_T\big|_{D/L}$ is the ratio of feedthrough-command power to total power, as given by Equation (29). The dimensionless function $\hat{S}_{cmd}(f_{\mathrm{chip}}T_{cmd})$ is given by:

$$\hat{S}_{cmd}(f_{\text{chip}}T_{cmd}) = \frac{1}{T_{cmd}} \cdot \max_{n} \begin{cases} S_{cmd}(f_{1,1}), & n = 1 \\ \sum_{k=0}^{\infty} P_{n,k}\, S_{cmd}(f_{n,k}), & 2 \le n \le 6 \end{cases} \tag{80}$$

Equation (80) is of the same form as Equation (73). The differences are that Equation (80) uses the command symbol period T_{cmd} and the one-sided, unity-power, power spectral density $S_{cmd}(\cdot)$ that is appropriate for command.

The curve-fits for $\hat{S}_{cmd}(f_{\text{chip}}T_{cmd})$ are of the same form as those for $\hat{S}_{tlm}(f_{\text{chip}}T_{tlm})$. Of course, these curve-fits use the product of the chip rate f_{chip} and the command symbol period T_{cmd}. For NRZ command symbols,

$$\hat{S}_{cmd}(f_{\text{chip}}T_{cmd}) \cong 0.090 + 1.88 \exp(-0.46\, f_{\text{chip}}T_{cmd}) \qquad \text{NRZ} \tag{81}$$

Whereas for bi-phase command symbols,

$$\hat{S}_{cmd}(f_{\text{chip}}T_{cmd}) \cong \begin{cases} 2 \cdot \sin^4(\pi f_{\text{chip}}T_{cmd}/4)/(\pi f_{\text{chip}}T_{cmd}/4)^2, & f_{\text{chip}}T_{cmd} \le 2.25 \\ 0.090 + 0.77 \exp(-0.20\, f_{\text{chip}}T_{cmd}), & f_{\text{chip}}T_{cmd} > 2.25 \end{cases} \tag{82}$$

The upper bound on K_{fth}, for NRZ command, is

$$\mathrm{K}_{fth} \le 2T_{cmd} \cdot \left.\frac{P_T}{N_0}\right|_{\mathrm{D/L}} \cdot \left.\frac{P_{fth}}{P_T}\right|_{\mathrm{D/L}} \qquad \text{NRZ} \tag{83}$$

$P_T/N_0|_{D/L}$ is the downlink total signal to noise spectral density ratio. $P_{fth}/P_T\big|_{D/L}$ is the ratio of feedthrough-command power to total power, as given by Equation (29). When the command symbol rate is large compared with the range-code chip rate (that is, when $f_{\text{chip}}T_{cmd} \ll 1$), this upper bound on K_{fth} is tight and the upper bound is a good approximation for K_{fth}.

The upper bound on K_{fth} for bi-phase command is

$$\mathrm{K}_{fth} \le 1.1 \cdot T_{cmd} \cdot \left.\frac{P_T}{N_0}\right|_{\mathrm{D/L}} \cdot \left.\frac{P_{fth}}{P_T}\right|_{\mathrm{D/L}} \qquad \text{bi-phase} \tag{84}$$

For bi-phase command when $f_{\text{chip}}T_{cmd} \ll 1$, the command-feedthrough interference to a range measurement may be negligible.

2.5.4 Range Measurement Error Due to Thermal Noise

The standard deviation σ_ρ of range measurement error, in meters rms, due to downlink thermal noise is given by

$$\sigma_\rho = \frac{c}{f_{RC} \cdot A_c \cdot R_1 \cdot \sqrt{32\pi^2 \cdot T \cdot (P_R/N_0)}} \tag{85}$$

where

c = speed of electromagnetic waves in vacuum, $299{,}792{,}458\ \mathrm{m/s}$

A_c= fractional loss of correlation amplitude due to frequency mismatch ($A_c \leq 1$)

R_1 = cross-correlation factor for the correlation against the range clock

T = range measurement integration time

f_{RC} = frequency of the range clock

$A_c = 1$ under the normal circumstances, in which the range clock is coherently related to the carrier. In the special case of non-coherent ranging, $A_c < 1$.

P_R/N_0, the ratio of the downlink ranging signal power to the downlink noise spectral density, is given by Equation (59) when there is no significant interference present or by Equation (60) when interference must be taken into account.

P_R, as it appears in P_R/N_0, is that portion of the power in the downlink ranging sidebands that is used in the range measurement, either in the correlation that determines the range measurement error or in the resolution of the ambiguity. The power ${R_1}^2 P_R$ is utilized in the correlation that determines the range measurement error. It may be noted that ${\sigma_\rho}^2$, the square of the standard deviation given in Equation (85), is inversely proportional to ${R_1}^2 P_R$. In the spectrum of the modulated downlink carrier, the power ${R_1}^2 P_R$ is evenly divided between the discrete spectral line f_{RC} hertz below the residual carrier and the discrete spectral line f_{RC} hertz above the residual carrier.

For the DSN and T4B codes, the standard deviation of range measurement error (meters) due to thermal noise is plotted in Figure 12 against the product $T \cdot (P_R/N_0)$, expressed in decibels: $10 \log(T \cdot P_R/N_0)$. These curves were calculated from Equation (85) using the cross-correlation factor R_1 given in Table 3 for the DSN range code and Table 4 for the T4B code. Also, the range clock was taken to be a 1-MHz sinewave and A_c was taken to be 1. The factor R_1 depends on the range code. For the DSN range code, $R_1 = 0.9544$. For the T4B code, $R_1 = 0.9387$. This difference is the reason the two curves in Figure 12 do not overlap.

The T2B code was designed to operate at smaller values of $T \cdot (P_R/N_0)$. For the T2B code, the standard deviation of range measurement error (meters) due to thermal noise is plotted in Figure 13. This curve was calculated from Equation (85) using the cross-correlation factor R_1 given in Table 5. The range clock was taken to be a 1-MHz sinewave, and A_c was taken to be 1. The factor P_R in the product $T \cdot (P_R/N_0)$ is that portion of the power in the downlink ranging sidebands that is used in the range measurement, either in the correlation that determines the range measurement error or in the resolution of the ambiguity.

The standard deviation of the two-way time delay σ_τ, in seconds, is related to σ_ρ, as given in Eq. (85), by

$$\sigma_\tau = \frac{2}{c} \cdot \sigma_\rho \tag{86}$$

The factor of 2 in Eq. (86) accounts for the fact that σ_ρ characterizes the error in the *one*-way range, while σ_τ characterizes the error in a *two*-way time delay. The standard deviation of the two-way phase delay σ_{RU}, as measured in range units, is related to σ_τ by

$$\sigma_{RU} = \begin{cases} \frac{f_S}{2} \cdot \sigma_\tau, & \text{S-band uplink} \\ \frac{221}{749} \cdot \frac{f_X}{2} \cdot \sigma_\tau, & \text{X-band uplink} \\ \frac{221}{2407} \cdot \frac{f_X}{2} \cdot \sigma_\tau, & \text{K-band uplink} \\ \frac{221}{3599} \cdot \frac{f_{Ka}}{2} \cdot \sigma_\tau, & \text{Ka-band uplink} \end{cases} \quad (87)$$

where f_S is the frequency of an S-band uplink carrier, f_X is the frequency of an X-band uplink carrier, f_K is the frequency of a K-band uplink carrier, and f_{Ka} is the frequency of a Ka-band uplink carrier.

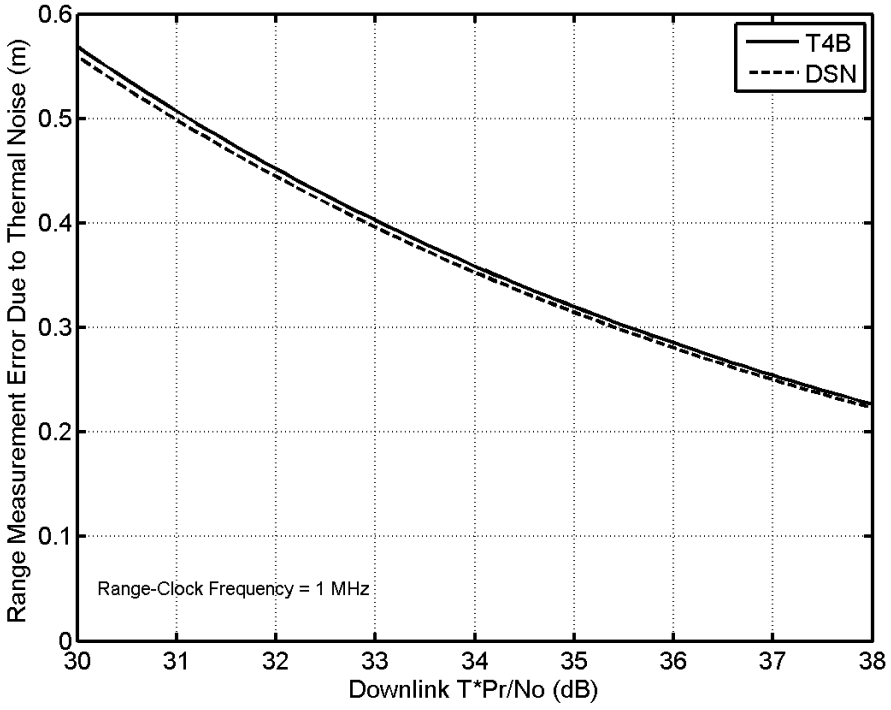

Figure 12. Standard Deviation of Range Measurement Error for the DSN and T4B Codes

2.5.4.1 Range Measurement Error for Turn-Around (Non-Regenerative) Ranging

For turn-around ranging, Equation (85) accounts for both uplink and downlink thermal noise. In this case, P_R is reduced by the effect of uplink noise and any command feedthrough. This can be understood from Equation (27) by noting that $P_R/P_T|_{D/L}$ depends on the rms phase deviations θ_r, θ_{cmd}, and θ_n.

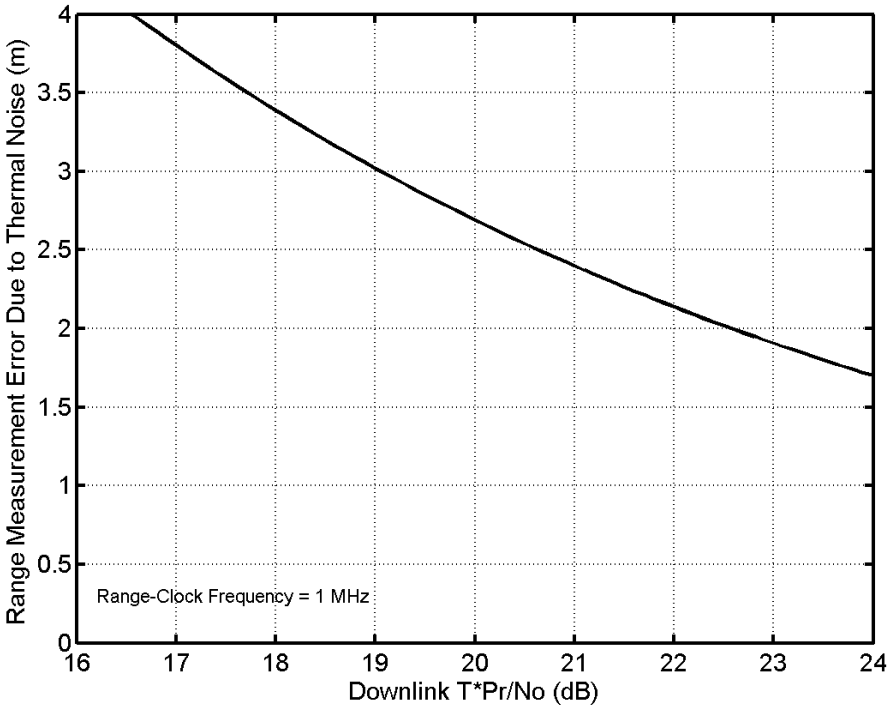

Figure 13. Standard Deviation of Range Measurement Error for the T2B Code

2.5.4.2 Range Measurement Error for Regenerative Ranging

For regenerative ranging, the standard deviation σ_{RR} of range measurement error, in meters rms, due to uplink and downlink thermal noise is given by

$$\sigma_{RR} = \sqrt{{\sigma_\rho}^2 + {\sigma_{\mathrm{U/L}}}^2} \tag{88}$$

${\sigma_\rho}^2$ is the square of the standard deviation σ_ρ of the range measurement error due to downlink thermal noise. σ_ρ is calculated from Equation (85). In the case of regenerative ranging, this calculation uses the $P_R/P_T|_{\mathrm{D/L}}$ that is defined in Equation (51). This (regenerative-ranging) $P_R/P_T|_{\mathrm{D/L}}$ contains no contribution from uplink thermal noise.

Uplink thermal noise causes phase jitter on the regenerated ranging signal. This phase jitter arises in the tracking loop that is part of the regeneration signal processing (Reference 5). This tracking jitter is a potential error source for the two-way range measurement. The standard deviation $\sigma_{\mathrm{U/L}}$ of range measurement error, meters rms, for this error source is given by

$$\sigma_{\mathrm{U/L}} = \frac{c}{4\pi R_1 f_{RC}} \sqrt{\frac{B_{RL}}{P_R/P_T|_{\mathrm{U/L}} \cdot P_T/N_0|_{\mathrm{U/L}}}} \tag{89}$$

where B_{RL} is the bandwidth of the loop that tracks the uplink range clock. The error $\sigma_{\mathrm{U/L}}$ only applies in the case of regenerative ranging. The range measurement error for a two-way, regenerative ranging measurement is computed as the root-sum-square of $\sigma_{\mathrm{U/L}}$ and σ_ρ, as indicated in Equation (88). For some missions it will be typical that $\sigma_{\mathrm{U/L}} \ll \sigma_\rho$, in which case σ_{RR} can be approximated as σ_ρ.

Regenerative ranging has better performance than turn-around ranging. A difference in bandwidth is the reason for this. With regenerative ranging, the bandwidth of the transponder's range-clock loop, B_{RL} in Equation (89), is typically small, perhaps a few hertz. With turn-around ranging, the bandwidth B_R of the transponder's ranging channel is typically about 1.5 MHz.

2.5.5 Probability of Acquisition

A correct determination of the range can only happen if the ambiguity is correctly resolved. This is accomplished with a set of correlations within the RRT between the received baseband ranging signal and local models of the component codes. A range measurement is successfully acquired when every code component is correctly acquired. The probability of acquisition P_{acq} for the range measurement is the product of the five probabilities P_n, $2 \le n \le 6$.

$$P_{\mathrm{acq}} = \prod_{n=2}^{6} P_n \tag{90}$$

P_n is the probability of acquiring the *n*-th component code ($2 \le n \le 6$). Each P_n is calculated by

$$P_n = \frac{1}{\sqrt{\pi}} \int_{-\infty}^{\infty} e^{-x^2} \left(\frac{1 + \mathrm{erf}\left(x + A_c\, R_n \sqrt{T \cdot (P_R/N_0)}\right)}{2} \right)^{\lambda_n - 1} dx \tag{91}$$

where λ_n and R_n are the code length (in chips) and cross-correlation factor for the *n*-th component code. Numerical integration is required to evaluate Equation (91). The error function $\mathrm{erf}(\cdot)$ is defined by

$$\mathrm{erf}(y) = \frac{2}{\sqrt{\pi}} \int_0^y e^{-t^2}\, dt \tag{92}$$

The value that Equation (90) gives for P_{acq} is, in general, greater than 0 and less than 1. P_{acq} is often characterized as a percentage (between 0% and 100%).

When interpreting Equation (91), it should be remembered that P_R is that portion of the power in the downlink ranging sidebands that is used in the range measurement. Not all of the power P_R is employed in acquisition (the resolution of the ambiguity). The power that helps with the code-component n correlation is ${R_n}^2 P_R$, where $2 \le n \le 6$.

Table 6 lists required values for $(A_c\, R_n)^2 \cdot T \cdot P_R/N_0$ (in decibels) as a function of λ_n (the code length) and P_n (the probability of acquiring the *n*-th component code). This table is based on Equation (91). The first column of Table 6 is $\log(P_n)$, where $\log(\cdot)$ is the common logarithm (the base-10 logarithm).

Table 6. Interpolation Table

Required $(A_c\, R_n)^2 \cdot T \cdot P_R/N_0$ (in decibels) for Given λ_n and P_n

$\log(P_n)$	$\lambda_n = 7$	$\lambda_n = 11$	$\lambda_n = 15$	$\lambda_n = 19$	$\lambda_n = 23$
-0.050	5.7	6.5	6.9	7.1	7.4
-0.040	6.2	6.9	7.2	7.5	7.7
-0.030	6.7	7.3	7.7	7.9	8.1
-0.020	7.4	7.9	8.3	8.5	8.7
-0.010	8.3	8.8	9.1	9.3	9.4
-0.009	8.4	8.9	9.2	9.4	9.5
-0.008	8.6	9.0	9.3	9.5	9.7
-0.007	8.7	9.2	9.4	9.6	9.8
-0.006	8.9	9.3	9.6	9.8	9.9
-0.005	9.1	9.5	9.8	9.9	10.1
-0.004	9.3	9.7	10.0	10.1	10.3
-0.003	9.6	10.0	10.2	10.4	10.5
-0.002	9.9	10.3	10.5	10.7	10.8
-0.001	10.5	10.8	11.0	11.1	11.3

Here is an example of how Table 6 can be used. If the desired P_n for a component code of length 19 is 0.99, then $\log(P_n) = -0.0044$. From Table 6, the decibel values 9.9 dB and 10.1 dB are found for $\log(P_n) = -0.005$ and $\log(P_n) = -0.004$, respectively. An interpolation suggests that $(A_c\, R_n)^2 \cdot T \cdot P_R/N_0$ must be about 10.0 dB in order to correctly acquire with probability $P_n = 0.99$ the component code having $\lambda_n = 19$. Of course, it is important to recall that $P_n = 0.99$ is not the probability of acquisition of the composite code. There are several component codes that must be correctly acquired before the range measurement is successfully acquired. P_{acq} is given by Equation (90), and it will be less than the value of any individual P_n.

For the DSN range code and the T4B code, P_{acq} is plotted in Figure 14 as a function of the product $T \cdot (P_R/N_0)$, in decibels: $10 \log(T \cdot P_R/N_0)$. For the T2B code, P_{acq} is plotted in Figure 15 as a function of the product $T \cdot (P_R/N_0)$, in decibels. The curves in these

two figures were calculated from Equations (90) and (91) using $A_c = 1$ and cross-correlation factors from Table 3, Table 4, and Table 5.

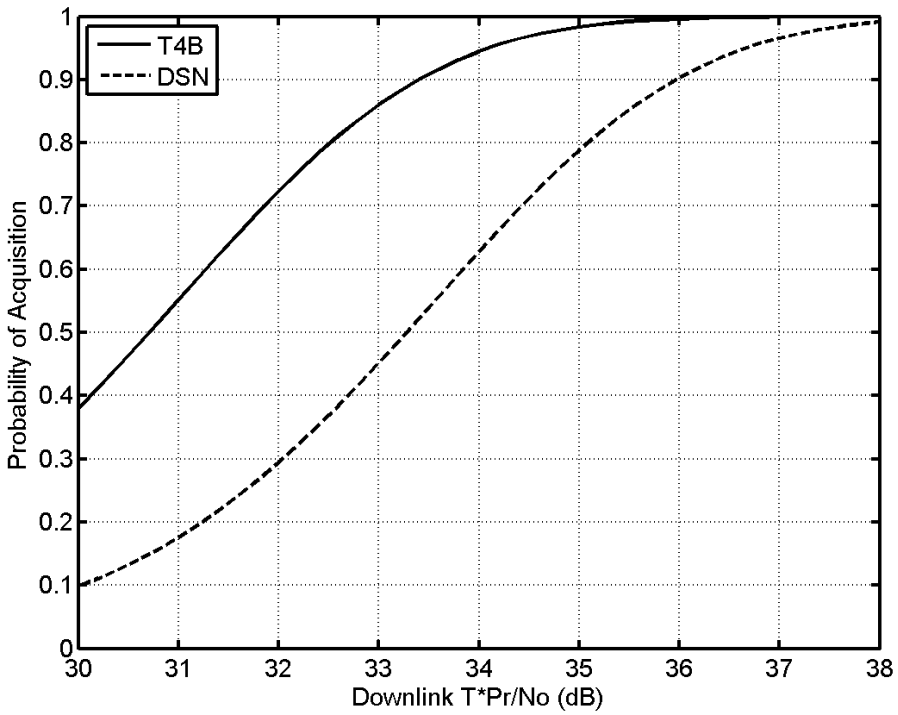

Figure 14. Probability of Acquisition for the DSN Range Code and the T4B Code

An approximation of P_{acq} may be calculated using the following curve fit:

$$P_{\text{acq}} = \begin{cases} c_3 Z^3 + c_2 Z^2 + c_1 Z + c_0, & Z_1 \le Z \le Z_2 \\ 1.00, & Z > Z_2 \end{cases} \tag{93}$$

where Z is the product $T \cdot (P_R/N_0)$ in units of decibels,

$$Z = 10 \log[T \cdot (P_R/N_0)] \quad \text{dB} \tag{94}$$

The parameters for the model of Equation (93) are given in Table 7. The correct set of parameters depends on the code (DSN range code, T4B, or T2B), as indicated in Table 7. The model of Equation (93) is not reliable for $Z < Z_1$ dB. For $Z > Z_2$ dB, the approximation $P_{\text{acq}} = 1$ may be used.

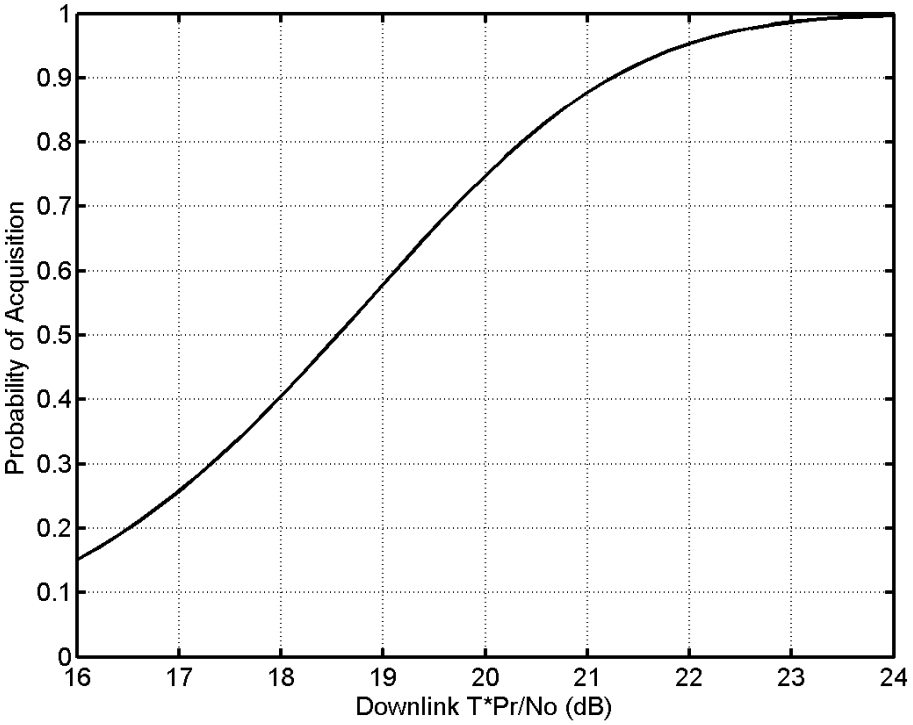

Figure 15. Probability of Acquisition for the T2B Code

Table 7. Parameters for Equation (93)

	DSN range code	T4B	T2B
Z_1	30 dB	28 dB	16 dB
Z_2	37 dB	35 dB	23 dB
c_3	-0.0039916	-0.0038441	-0.0037013
c_2	0.400534	0.356736	0.208431
c_1	-13.2253	-10.8645	-3.7427
c_0	144.154	109.048	21.833

Comparing Figure 12 and Figure 14, it becomes clear that the DSN range code was designed to give a σ_ρ of about 0.2 to 0.3 meter when the product $T \cdot P_R/N_0$ is just large enough (about 37 to 38 dB) to assure a high probability of acquisition. The T4B code has better acquisition performance than the DSN range code. Comparing Figure 13 and Figure 15, it can

be seen that the T2B code achieves a high P_{acq} for considerably smaller $T \cdot P_R/N_0$, but the price paid is a larger σ_ρ, about 2 meters.

2.5.6 Processing a Set of Range Measurements

For a given PN range code, a minimum $T \cdot (P_R/N_0)$ product is needed to achieve a high P_{acq}, and there is an approximate range measurement error (standard deviation) corresponding to this $T \cdot (P_R/N_0)$. In the example discussed above, the DSN range code ordinarily requires that $T \cdot (P_R/N_0)$ be about 37 to 38 dB in order to assure a high P_{acq}, and the corresponding range measurement error is about 0.2 to 0.3 meter.

Sometimes the available $T \cdot (P_R/N_0)$ is smaller than the minimum value for which a range code was designed to work. It is still possible to acquire range measurements with the correct resolution of the ambiguity even under the circumstance of a low $T \cdot (P_R/N_0)$. This is accomplished by using a large set of range measurements (obtained from one station tracking one spacecraft).

Reference 6 describes the "Plurality Voting Method" for accomplishing range acquisitions for a large measurement data set when $T \cdot (P_R/N_0)$ is low. This method employs range residuals for the given set of range measurements. A range residual is the difference between the measured two-way delay and the predicted two-way delay, where the predicted value is computed from a spacecraft ephemeris. Doppler velocity residuals can also be used. The Plurality Voting Method, making use of a large set of range measurements, increases the acquisition probability beyond that given in Eq. (90). This method does not, however, improve the standard deviation of acquired range measurements. The Plurality Voting Method has value in scenarios where $T \cdot (P_R/N_0)$ is adequate for the required range accuracy (standard deviation) but is inadequate (in the absence of this special method) for the required acquisition probability.

2.5.7 Comparison of PN Ranging and Sequential Ranging

It is instructive to compare the performance of turn-around PN ranging with sequential ranging (Reference 7). For both techniques, a minimum integration time T can be calculated as a function of P_R/N_0 for a given range measurement error σ_ρ (due to thermal noise) and a given P_{acq}. For the purpose of the present comparison, σ_ρ is taken to be 0.2 m and P_{acq} is taken to be 0.99. Furthermore, the range-clock frequency f_{RC} is taken to be 1 MHz.

For the analysis presented here, the minimum T is calculated for the DSN range code by finding, for a given P_R/N_0, the smallest T that satisfies the two constraints: $\sigma_\rho < 0.2$ m, as calculated with Equation (85), and $P_{\text{acq}} > 0.99$, as calculated with Equations (90) and (91).

For sequential ranging, the number of sinewaves in the sequence is taken to be 20; this gives an ambiguity resolution of 78,590 km, comparable with the 75,660 km ambiguity resolution offered by the DSN range code. The minimum T for sequential ranging is the minimum cycle time consistent with a range error (due to thermal noise) of 0.2 m and a probability of acquisition of 0.99. The cycle time includes the range-clock integration time T_1 plus 19 times the ambiguity integration time T_2 plus the required deadtime seconds.

Figure 16 shows the ratio of the minimum T (cycle time) for sequential ranging to the minimum T (integration time) for PN ranging as a function of P_R/N_0. This figure is intended

as a performance comparison of sequential ranging and turn-around PN ranging. The underlying assumption is that P_R/N_0 is approximately the same for these two ranging techniques for a given set of link parameters.

In principle, a plot like this also applies to regenerative PN ranging. However, P_R/N_0 will not be the same for regenerative PN ranging and (non-regenerative) sequential ranging. In general, it is expected that regenerative PN ranging will out-perform (non-regenerative) sequential ranging.

The results of Figure 16 suggest that sequential ranging has a small performance advantage over turn-around PN ranging for small P_R/N_0 (less than about 12 dB-Hz for the parameters used here) but that PN ranging has a performance advantage for P_R/N_0 larger than this. When the sequential ranging minimum T is larger than the PN ranging minimum T (that is, when P_R/N_0 is larger than about 12 dB-Hz), the choice to use PN ranging means that more range measurements can be made in a given period than can be made with sequential ranging.

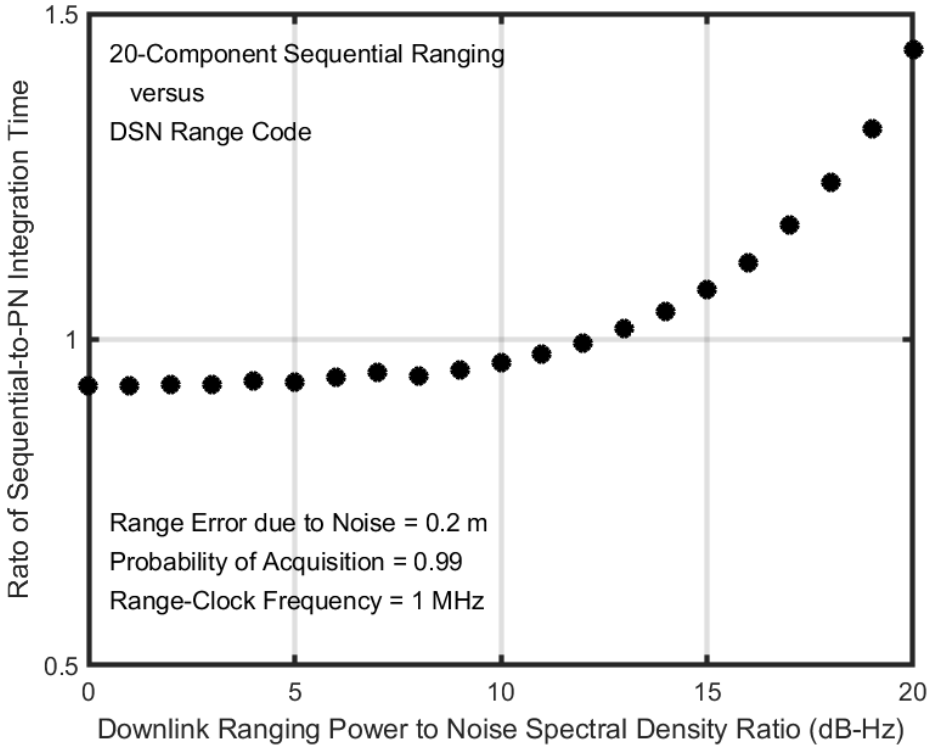

Figure 16. Comparison of Sequential Ranging and PN Ranging

PN ranging has an operational advantage over sequential ranging. With sequential ranging, a large increase in the RTLT during the tracking pass forces a measurement restart. This is not an issue for PN ranging. The PN range code has a period of approximately 0.5 second when the range clock has its typical frequency of about 1 MHz. (The measurement integration time T is larger, as the measurement comprises multiple periods of the PN range code.) With PN ranging, the downlink can start processing at any 1-second boundary.

2.5.8 Comparison of the Different PN Ranging Techniques

There are three PN range codes supported by the Deep Space Network: the heritage DSN range code and the T4B and T2B range codes. The CCSDS recommends the T4B and the T2B range codes. These three range codes are all built from the same set of component PN codes. (See Table 2.) The differences between these three range codes arise because each combines the component PN codes in its own way. For all three of these range codes (DSN, T4B, and T2B), the range-clock equals one-half of the chip rate. A turn-around ranging channel within a spacecraft transponder is compatible with all three of these range codes, assuming its bandwidth is sufficiently large.

The DSN range code and the T4B range code offer similar range-measurement precision as a function of downlink $T \cdot P_R/N_0$. (See Figure 12.) However, the T4B range code outperforms the DSN range code in acquisition. For example, the DSN range code requires that the downlink $T \cdot P_R/N_0$ be 37.9 dB for an acquisition probability of 99%, whereas the T4B range code only requires 35.3 dB for the same acquisition probability. (See Figure 14.)

Compared to the DSN and T4B range codes, the T2B range code can be reliably acquired with a much smaller downlink $T \cdot P_R/N_0$. For example, the T2B range code only requires a downlink $T \cdot P_R/N_0$ of 23.2 dB for an acquisition probability of 99%. (See Figure 15.) The disadvantage of the T2B range code is that it cannot achieve the same range-measurement precision as the other two range codes. (Compare Figure 12 and Figure 13.)

Regenerative ranging offers, in principle, a performance improvement over non-regenerative (turn-around) ranging for a given range code. Whether this performance improvement is significant depends on the link parameters. The performance advantage of regenerative ranging comes at the expense (to the mission) of needing special regenerative signal processing in the ranging channel of the transponder. The signal processing in a regenerative-ranging transponder is specific to the exact range code being used. Within the Deep Space Network, the processing of a range measurement is independent of whether the transponder employs regenerative or non-regenerative ranging.

2.5.9 Non-Coherent Operation

A non-coherent ranging technique has been described in Reference 8. For the sake of economy, this technique employs a transceiver, rather than a transponder, at the spacecraft. With such a technique, the downlink carrier is not coherent with the uplink carrier, and the downlink range clock is not coherent with the downlink carrier. This means that there will ordinarily be a frequency mismatch between the received downlink range clock and its local model. This mismatch is to be minimized by Doppler compensation of the uplink carrier, but it will not be possible, in general, to eliminate completely the frequency mismatch. With this non-coherent technique, range measurement performance will not be as good as that which can be achieved with coherent operation using a transponder. Nonetheless, non-coherent range measurement performance is expected to be adequate for some mission scenarios.

The frequency mismatch inherent in non-coherent ranging has two effects on performance. One is a loss A_c of correlation amplitude, which increases the thermal noise contribution to measurement error. The other is a direct contribution to range measurement error. This direct contribution is much the more important of these two effects.

The loss of correlation amplitude is represented by A_c where $0 < A_c < 1$. The standard deviation σ_ρ of range measurement error due to thermal noise is given by Equation (85), and the probability of acquisition (considering the effect of thermal noise) is given by Equations (90) and (91). The amplitude loss factor A_c is, for non-coherent operation, given by

$$A_c = |\mathrm{sinc}(2\Delta f_{RC} T)| \tag{95}$$

where Δf_{RC} is the frequency mismatch between the received range clock and its local model. The function $\mathrm{sinc}(\cdot)$ is defined by Equation (56). For coherent operation, $\Delta f_{RC} = 0$ and $A_c = 1$.

The direct contribution of frequency mismatch to range measurement error is given by

$$\text{range error due to } \Delta f_{RC} = \frac{c}{4} \cdot \frac{\Delta f_{RC}}{f_{RC}} \cdot T, \qquad \text{m} \tag{96}$$

The range error given by Eq. (96) is in meters (with c in m/s, T in seconds, and with Δf_{RC} and f_{RC} sharing the same units). It is worth noting that this measurement error is directly proportional to both the fractional frequency mismatch $\Delta f_{RC}/f_{RC}$ and the measurement integration time T. The fractional frequency error will, in general, comprise two terms: a fractional frequency error due to uncertainty in the spacecraft oscillator frequency and a fractional frequency error due to imperfect uplink Doppler predicts.

Non-coherent ranging measurements should be done with regenerative ranging using PN signals. The reason for this follows. The direct error contribution due to frequency mismatch is directly proportional to the measurement integration time, as can be seen in Equation (96). So, for non-coherent operation, it is important to make T as small as possible. This is achieved with regenerative ranging, and regenerative ranging is only available with a PN ranging signal.

With non-coherent operation, the range error due to frequency mismatch increases with T and the range error due to thermal noise decreases with T. Therefore, it is important to seek an optimal value for T, in order to get the best possible performance. Reference 8 offers guidance in this matter.

2.6 Range Corrections

Range is defined to be the distance from the reference point on the DSS antenna to the reference point on the spacecraft antenna. The reference point of a DSS antenna is the intersection of the azimuth and elevation axes. When the two-way time delay is measured, the result includes more than just the two-way delay between the reference points of the DSS and spacecraft antennas. The measured two-way delay also includes station delay and spacecraft delay. These extra delays must be determined through calibration and then removed from the measured two-way time delay. The spacecraft delay is measured during DSN compatibility testing prior to launch. The station delay is determined in two parts: the DSS delay and the Z-correction.

A range measurement (that has not yet been corrected) provides the two-way delay through the station uplink path, starting from the USG, to and from the spacecraft, and through the station downlink path, ending in the RRT. Figure 17 illustrates the two-way signal

path at the station. It is necessary to determine the uplink station delay for the path from the USG to the antenna reference point, to determine the downlink station delay for the path from the antenna reference point to the RRT, and to remove these delays from the measured two-way delay.

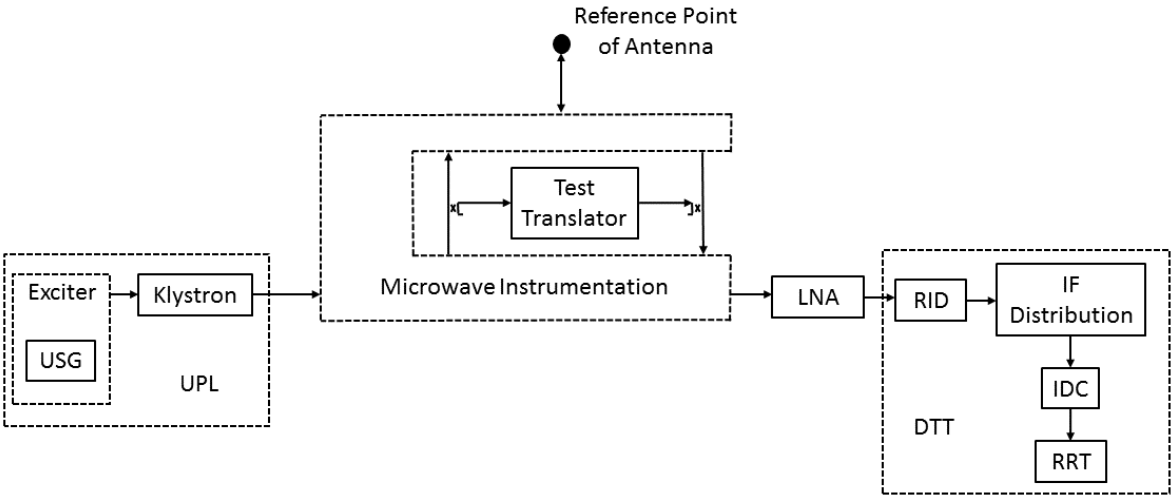

Figure 17. DSS Delay Calibration

2.6.1 DSS Delay

The DSS delay is obtained by a calibration that mimics an actual two-way range measurement, except that the signal path lies entirely within the station. A portion of the uplink carrier is diverted through a coupler to a test translator. The test translator shifts the carrier to the downlink frequency (while not altering the modulation) and feeds this frequency-shifted carrier to a coupler that places it on the downlink path within the station. The DSS delay contains most of the station delay. To be precise, the DSS delay comprises the delay from the USG to the ranging coupler on the uplink, the delay through the test translator (and its cables), and the delay from the ranging coupler on the downlink to the RRT.

Figure 17 is a somewhat abstract representation of the configuration. The microwave instrumentation shown in this figure is not an official subsystem, rather it is a conceptual grouping of microwave signal paths and microwave devices. On the uplink, the uplink carrier that is output from the klystron passes through the microwave instrumentation on its way to the reference point of the antenna. On the downlink, the downlink passes through the microwave instrumentation on its way to the LNA. Along the uplink path, a portion of the uplink carrier is coupled to the test translator. The portion of the carrier that has been frequency shifted to the downlink band inside the test translator is then coupled to the downlink path. The specific details of the microwave instrumentation are generally different at different DSSs and for different bands within a given DSS. Modules 101, 103 and 104 should be consulted for those details.

The DSS delay is station and configuration dependent. It should be measured for every ranging pass. This measurement is called precal for pre-track calibration and postcal for post-track calibration. The former is done at the beginning of a ranging pass; the latter is only

needed when there is a change in equipment configuration during the track or precal was not performed due to a lack of time.

The DSS delay varies significantly as a function of carrier frequency. This is illustrated in Figure 18 for an X-band (uplink and downlink) calibration at DSS 63. The vertical axis on this plot is the DSS delay, labeled STDL in this plot. The difference between the largest and smallest delays over the 8400—8450 MHz band is about 18 ns in this case. On both the lower and upper ends of this band, the rise in station delay originates in the klystron on the uplink side of the station. The ripple in the station delay arises from impedance mismatches; every transmission line that has some mismatch at both ends will introduce ripple in the group delay.

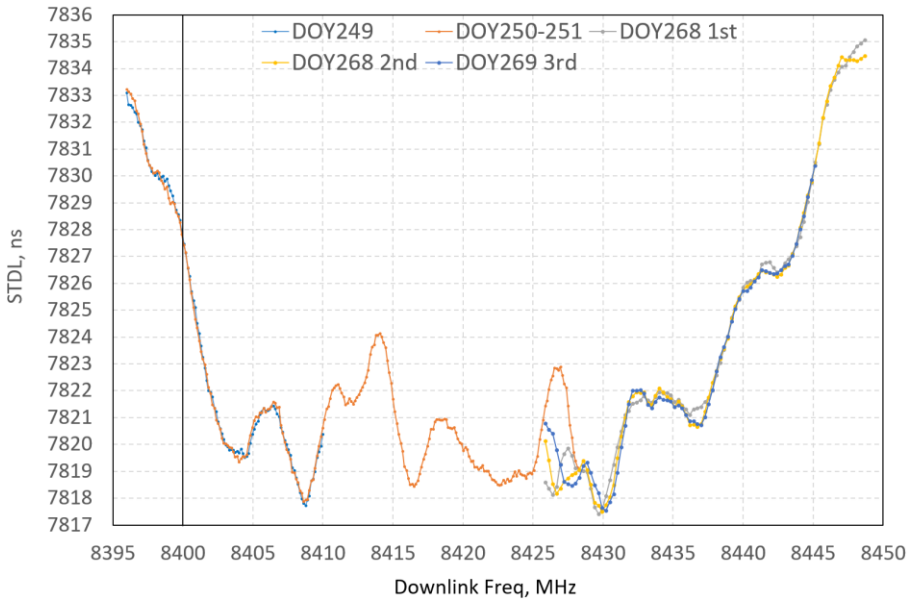

Figure 18. DSS Delay as a Function of Downlink Frequency

2.6.2 Z-Correction

The DSS delay itself must be corrected. This is accomplished with the Z-correction. The DSS delay includes the delay through the test translator (and its cables), but the test translator is not in the signal path of an actual range measurement. Moreover, the DSS delay does not include, but should include, the delays between the ranging couplers and the antenna reference point.

The Z-correction is defined as the delay through the test translator (and its cables) minus the uplink and downlink delays between the ranging couplers and the antenna reference point. The DSS delay minus the Z-correction therefore gives the delay between the USG and the antenna reference point plus the delay between the antenna reference point and the RRT. This is exactly the quantity that must be subtracted from a range measurement in order to produce a two-way delay relative to the antenna reference point.

The test translator delay is measured by installing a zero delay device (ZDD) in place of the test translator. Since the ZDD delay is measured in the laboratory, the signal delay contributed by the test translator can be calculated to a known precision. This measurement is made approximately once each year or when there are hardware changes in this portion of the signal path. The delays between the ranging couplers and the antenna reference point are stable and need not be updated often; they are determined by a combination of calculation and measurement.

2.7 Total Error for Range Measurement

Several error sources contribute to the total error for a range measurement. For two-way range measurement, the two most important error sources are typically thermal noise and station calibration error. The error due to thermal noise is discussed in Section 2.5. The error in calibrating and removing the station delay is often the dominant error source for two-way ranging. For two-way range measurements in the X band, there is typically about 6 ns of station calibration error in the two-way delay, corresponding to a (one-way) range error of about 1 meter.

The error in calibrating and removing the spacecraft delay is stable for a given spacecraft and a given band pairing (for example, X band on the uplink and X band on the downlink). The orbit determination program can, given enough range measurements for this spacecraft and band pairing, solve for this error.

There are error contributions, usually small compared to the station calibration error, due to the passage of the uplink and downlink through the troposphere, ionosphere and solar corona (Reference 9). When the angle between the sun and the spacecraft, as seen from the station, is small and the spacecraft is beyond the sun, the error contribution from the solar corona can become the dominant contributor to error in the range measurement.

For three-way ranging (in which one station transmits the uplink and a second station receives the downlink), the total delay measurement error is larger than for two-way. There are two reasons for this. First, there is a clock offset between the transmitting and receiving stations. Second, the calibration of the station delays is more difficult to achieve accurately in this case.

Appendix: Glossary of Parameters

$P_T/N_0\|_{\mathrm{U/L}}$	ratio of uplink total power to noise spectral density, Hz
$P_C/P_T\|_{\mathrm{U/L}}$	ratio of uplink residual-carrier to total power
$P_R/P_T\|_{\mathrm{U/L}}$	ratio of uplink ranging-signal to total power
$P_D/P_T\|_{\mathrm{U/L}}$	ratio of uplink command-signal to total power
$P_T/N_0\|_{\mathrm{D/L}}$	ratio of downlink total power to noise spectral density, Hz
$P_C/P_T\|_{\mathrm{D/L}}$	ratio of downlink residual-carrier to total power
$P_R/P_T\|_{\mathrm{D/L}}$	ratio of downlink ranging-signal to total power
$P_D/P_T\|_{\mathrm{D/L}}$	ratio of downlink telemetry to total power
$P_{fth}/P_T\|_{\mathrm{D/L}}$	ratio of command-feedthrough power to total power on downlink
$E_S/N_0\|_{\mathrm{D/L}}$	ratio of telemetry symbol energy to noise spectral density
P_R/N_0	ratio of downlink ranging-signal power to noise spectral density, Hz
P_k/P_T	ratio of discrete spectral line power to total power
Z	$T \cdot (P_R/N_0)$ in decibels
ρ_ρ	ranging signal-to-noise ratio in transponder's ranging channel
ρ_{cmd}	command-feedthrough signal-to-noise ratio in transponder's ranging channel
$C_R(B_R T_{cmd})$	fraction of command-signal power passing through ranging channel
T_{cmd}	command symbol period, s
T_{tlm}	telemetry symbol period, s
B_R	noise-equivalent bandwidth of transponder's ranging channel, Hz
B_{RL}	noise-equivalent bandwidth of uplink code-tracking loop, Hz
T	integration time for range measurement, s
T_c	chip period, s
f_{chip}	chip rate, Hz
f_{RC}	range-clock frequency, Hz
f_C	frequency of residual carrier, Hz
f_S	S-band carrier frequency, Hz

f_X	X-band carrier frequency, Hz
f_K	K-band carrier frequency, Hz
f_{Ka}	Ka-band carrier frequency, Hz
Δf_{RC}	difference between the received range-clock frequency and its local model, Hz
A/B	rational factor that, together with the uplink carrier frequency, sets the chip rate
c	speed of electromagnetic waves in vacuum, m/s
λ_n	period of n-th component code
L	length of composite code
R_n	cross-correlation factor of code component n against composite code
A_c	fractional loss of correlation amplitude due to non-coherent frequency mismatch
ϕ_r	phase deviation of uplink carrier by ranging signal, rad rms
ϕ_{cmd}	phase deviation of uplink carrier by command signal, rad rms
θ_{rs}	phase deviation of downlink carrier by ranging signal (strong signal), rad rms
θ_r	phase deviation of downlink carrier by ranging signal, rad rms
θ_{cmd}	phase deviation of downlink carrier by command feedthrough, rad rms
θ_n	phase deviation of downlink carrier by noise, rad rms
θ_{tlm}	telemetry modulation index, rad
$S_{cmd}(\phi_{cmd})$	suppression factor on uplink due to command
$M_{cmd}(\phi_{cmd})$	modulation factor on uplink for command
$S_{fth}(\theta_{cmd})$	suppression factor on downlink due to command feedthrough
$M_{fth}(\theta_{cmd})$	modulation factor on downlink for command feedthrough
$S_{tlm}(\theta_{tlm})$	suppression factor on downlink due to telemetry
$M_{tlm}(\theta_{tlm})$	modulation factor on downlink for telemetry
P_n	probability of acquiring the n-the component code
P_{acq}	probability of acquisition
σ_ρ	standard deviation of range measurement error due to downlink noise, m
$\sigma_{\mathrm{U/L}}$	standard deviation of range measurement error due to uplink noise, m

σ_{RR}	standard deviation of range measurement error due to all noise, m
σ_{τ}	standard deviation of two-way delay, s
σ_{RU}	standard deviation of the two-way phase delay, RU
Γ_Q	factor by which downlink noise floor increases in quadrature receiver channel
K_{NQ}	contribution to Γ_Q from uplink noise and downlink intermodulation products
K_{tlm}	contribution to Γ_Q from telemetry interference
K_{fth}	contribution to Γ_Q from feedthrough command interference
$P_{NQ}/P_T\big\vert_{\mathrm{D/L}}$	ratio of power from K_{NQ} sources to total power on downlink
$S_{tlm}(f)$	one-sided, unity-power, power spectral density of telemetry, 1/Hz
$S_{cmd}(f)$	one-sided, unity-power, power spectral density of command, 1/Hz
$\hat{S}_{tlm}(\cdot)$	maximum of weighted average of $S_{tlm}(f)$, normalized by T_{tlm}
$\hat{S}_{cmd}(\cdot)$	maximum of weighted average of $S_{cmd}(f)$, normalized by T_{cmd}
$f_{n,k}$	frequency of spectral line at frequency index k for component PN code n, Hz
$P_{n,k}$	relative power of spectral line at frequency index k for component PN code n
$\tilde{C}_n(k)$	DFT of component PN code n, as calculated from λ_n samples

References

1. J. B. Berner, S. H. Bryant, and P. W. Kinman, “Range Measurement as Practiced in the Deep Space Network,” *Proceedings of the IEEE*, Vol. 95, No. 11, November 2007.
2. Consultative Committee for Space Data Systems, "Pseudo-Noise (PN) Ranging Systems," CCSDS 414.1-B-2, February 2014.
3. P. W. Kinman and J. B. Berner, “Two-Way Ranging During Early Mission Phase,” *2003 IEEE Aerospace Conference*, March 8-15, 2003, Big Sky, MT.
4. J. L. Massey, G. Boscagli, and E. Vassallo, "Regenerative Pseudo-Noise (PN) Ranging Sequences for Deep-Space Missions," *Int. J. Satellite Communications and Networking*, Vol. 25, No. 3, pp. 285-304, May/June 2007.
5. J. B. Berner, J. M. Layland, P. W. Kinman, and J. R. Smith, “Regenerative Pseudo-Noise Ranging for Deep-Space Applications,” *TMO Progress Report 42-137*, Jet Propulsion Laboratory, Pasadena, CA, May 15, 1999.
6. J. R. Jensen, “A Plurality Voting Method for Acquisition of Regenerative Ranging Measurements,” *2013 IEEE Aerospace Conference*, March 2-9, 2013, Big Sky, MT.
7. J. B. Berner and S. H. Bryant, “Operations Comparison of Deep Space Ranging Types: Sequential Tone vs. Pseudo-Noise,” *2002 IEEE Aerospace Conference*, March 9-16, 2002, Big Sky, MT.
8. M. K. Reynolds, M. J. Reinhart, R. S. Bokulic, and S. H. Bryant, “A Two-Way Noncoherent Ranging Technique for Deep Space Missions,” *2002 IEEE Aerospace Conference*, March 9-16, 2002, Big Sky, MT.
9. C. L. Thornton and J. S. Border, *Radiometric Tracking Techniques for Deep-Space Navigation*, Monograph 1 of the *Deep-Space Communications and Navigation Series*, Jet Propulsion Laboratory, Pasadena, CA, 2000.